

Geometry-Preserving Encoder/Decoder In Latent Generative Models

Wonjun Lee

Institute for Mathematics and Its Applications, University of Minnesota

LEE01273@UMN.EDU

Riley C. W. O’Neill

Department of Mathematics, University of Minnesota

ONEIL571@UMN.EDU

Dongmian Zou

Zu Chongzhi Center for Mathematics and Computational Sciences, Duke Kunshan University

DONGMIAN.ZOU@DUKE.EDU

Jeff Calder

Department of Mathematics, University of Minnesota

JWCALDER@UMN.EDU

Gilad Lerman

Department of Mathematics, University of Minnesota

LERMAN@UMN.EDU

Abstract

Generative modeling aims to generate new data samples that resemble a given dataset, with diffusion models recently becoming the most popular generative model. One of the main challenges of diffusion models is solving the problem in the input space, which tends to be very high-dimensional. Recently, solving diffusion models in the latent space through an encoder that maps from the data space to a lower-dimensional latent space has been considered to make the training process more efficient and has shown state-of-the-art results. The variational autoencoder (VAE) is the most commonly used encoder/decoder framework in this domain, known for its ability to learn latent representations and generate data samples. In this paper, we introduce a novel encoder/decoder framework with theoretical properties distinct from those of the VAE, specifically designed to preserve the geometric structure of the data distribution. We demonstrate the significant advantages of this geometry-preserving encoder in the training process of both the encoder and decoder. Additionally, we provide theoretical results proving convergence of the training process, including convergence guarantees for encoder training, and results showing faster convergence of decoder training when using the geometry-preserving encoder.

Keywords: Generative modeling, latent diffusion model, geometry-preserving encoder, autoencoder, isometric map

1 Introduction

Autoencoders have long been recognized for their capability of representing data in low-dimensional spaces thanks to their encoder-decoder structures, and have been used widely since early dates of deep learning (Kramer, 1991; Bengio et al., 2013). More recently, latent diffusion models (Vahdat et al., 2021; Rombach et al., 2022) have attained remarkable success in generative tasks by doing diffusion in the latent spaces of autoencoders, significantly reducing the computational cost of diffusion models while maintaining high-quality image synthesis (Podell et al., 2023). In particular, Rombach et al. (2022) pointed out that using a pre-trained, regularized encoder/decoder module simplifies the training process compared to training the encoder/decoder and score-based prior simultaneously. However, the task

of training this regularized encoder/decoder itself – equivalent to training a Variational Autoencoder (VAE) – has its own challenges. Furthermore, its training process is not yet fully understood and often exhibits instabilities.

In the VAE framework, the encoder and decoder are optimized together using the Evidence Lower Bound (ELBO) loss, which combines a reconstruction loss term with a Kullback-Leibler (KL) divergence term to enforce a prior constraint. Balancing these two terms is crucial for the quality of VAE training results, but achieving this balance is known to be difficult (Lin et al., 2019; Asperti and Trentin, 2020; Alemi et al., 2018; Mathieu et al., 2019). Moreover, the KL divergence does not take into account the geometric structure of the underlying data space. It measures the difference between the distributions without considering how the structure among points in the data space is maintained in the latent space. This may lead to loss of information in the latent representation. Indeed, it is well known that VAEs suffer from so-called “posterior collapse” (Wang et al., 2021b), where the latent representation bends too much towards the prior distribution and discards important information about the data.

To address these challenges and achieve a latent representation that preserves essential data information, we propose a geometry-preserving encoder/decoder (GPE) model. Our approach involves learning a Gromov-Monge embedding as the encoder, followed by training the decoder based on reconstruction. The GPE framework offers provable theoretical properties concerning training loss and stability. Our specific contributions are as follows:

- We propose a new encoder/decoder framework that is primarily designed to preserve geometric structure in the data. The encoder and decoder are trained sequentially, rather than jointly, and are trained independently from downstream components such as diffusion models. Sequential training not only simplifies implementation but also facilitates theoretical analysis (Chapter 3).
- For the encoder, we theoretically show that the stability of training improves as the loss decreases, by proving the increasing convexity of the loss function. For the decoder, we demonstrate that as the encoder adheres more closely to the geometry-preserving condition, the stability and convergence rate for training the decoder both improve (Section 4).
- We provide upper bounds for the Wasserstein distance between the true distribution and the generated distribution, which serves as a measure for the performance of the GPE-based latent generative models, where the bounds are functions of the optimization objective of the GPE encoder, the reconstruction loss, and the distance between the embedded distribution and the pushforward distribution from the latent distribution (Section 5).
- We demonstrate through extensive experiments that GPE performs better and converges faster than VAE in reconstruction tasks. Moreover, due to its superior performance in reconstruction tasks, GPE also shows superior performance in generation tasks for certain datasets, specifically CelebA (Section 7)

1.1 Related works

1.1.1 ENCODER-DECODER FRAMEWORK FOR GENERATIVE TASKS

Encoder-decoder frameworks have been pivotal in generative modeling. Variational Autoencoders (VAEs) (Kingma and Welling, 2014) encode data into a low-dimensional latent space, and use the decoder for generation. Although VAEs are not capable of generating high-quality images, they can be improved by carefully designing the latent space. A well-known example is the Vector Quantized-VAE (VQ-VAE) (Van Den Oord et al., 2017). Learning the latent distribution also benefits other types of generative models. For instance, it can alleviate mode collapse in Generative Adversarial Networks (GANs) (Larsen et al., 2016; Srivastava et al., 2017; Gao et al., 2020; Makkuva et al., 2020). More recently, encoder-decoder structures have been used in diffusion models to improve sample efficiency (Pandey et al., 2021; Wang et al., 2021a; Vahdat et al., 2021; Gu et al., 2022; Rombach et al., 2022; Dao et al., 2023; Kim et al., 2024a).

1.1.2 GEOMETRY-PRESERVING EMBEDDINGS

Recent works have studied encoders whose latent representations preserve the structures of input data. For instance, Falorsi et al. (2019); Connor et al. (2021); Chen et al. (2021); Huh et al. (2024); Kim et al. (2024b) considered the manifold of the latent space data for recovering low-dimensional geometry in the data space. Meanwhile, Kato et al. (2020); Gropp et al. (2020); Lee et al. (2022) focused on constructing local isometries between the input and latent spaces. In contrast, our geometry-preserving property reveals a provably approximate global isometry.

The structural difference can be quantified using the Gromov-Wasserstein distance (Mémoli, 2011; Peyré et al., 2016; Alvarez-Melis and Jaakkola, 2018; Xu et al., 2019a,b; Li et al., 2022), which has recently found application in neural generative models (Bunne et al., 2019; Titouan et al., 2019; Nakagawa et al., 2023). More recently, Lee et al. (2023) and Yang et al. (2024) discovered that the Gromov-Monge variant of the Gromov-Wasserstein distance serves as an effective regularization term for preserving the geometry of data representations. Our work also utilizes the Gromov-Monge distance. However, we train the encoder entirely based on this distance rather than using it as a regularization term. Thanks to this algorithmic difference, we have theories that directly address training stability and efficiently, as well as an upper bound for the generated distribution. The theories are different from previous works.

1.2 Structure of the paper

This paper is organized as follows. We begin in Section 2, where we detail the underlying assumptions that are crucial for the theoretical analysis. In Section 3, we introduce the geometry-preserving encoder/decoder (GPE) framework and contrast it with the Variational Autoencoder (VAE) framework. This section highlights the key differences in how each framework handles the embedding of data distributions into latent space, with a focus on the preservation of geometric structure.

Section 4 presents our theoretical analysis of the GPE framework, including the efficiency of computing the GPE encoder and decoder from the proposed formulations. We provide

detailed proofs and discuss the implications of these results. Following this, in Section 5, we briefly review the latent diffusion model and extend our theoretical analysis to the GPE-based latent diffusion model. Here, we demonstrate how the framework’s performance, as measured by the Wasserstein distance between the underlying and generated distributions, improves with enhanced geometry-preserving properties of the encoder and decoder.

In Section 6, we outline the algorithm for computing the GPE encoder and decoder. Section 7 follows with numerical results that validate the theoretical findings from the preceding sections. We present experiments on both artificial datasets and real-world datasets, such as MNIST and CelebA-HQ (256×256), and compare the performance of the GPE framework with the VAE framework in both reconstruction and generation tasks.

Finally, the paper concludes in Section 8, where we summarize the key findings, discuss the broader implications of our results, and suggest potential directions for future research.

2 Assumptions

In this section, we establish notations and assumptions essential for our study. The probability distribution μ , which is absolutely continuous with respect to Lebesgue measure \mathcal{L} on a k -dimensional compact submanifold \mathcal{M} in \mathbb{R}^D (where $k \ll D$) such that there exists a measurable function $\rho : \mathcal{M} \rightarrow \mathbb{R}$ satisfying $d\mu(x) = \rho(x)d\mathcal{L}(x)$. Assume ρ is bounded above and below by positive constants ρ_{\min} and ρ_{\max} , ensuring

$$0 < \rho_{\min} \leq \rho(x) \leq \rho_{\max}, \quad \forall x \in \mathcal{M}. \quad (1)$$

Denote by $\nu = \mathbb{P}(\mathbb{R}^d)$ the latent distribution, specifically chosen as the d -dimensional standard normal distribution with $d \geq k$. Define $T : \mathcal{M} \rightarrow \mathbb{R}^d$ as an embedding map or an encoder, and $T_{\#}\mu$ as the pushforward measure defined by $T_{\#}\mu(A) = \rho(T^{-1}(A))$ for all measurable subsets $A \subset \mathbb{R}^d$. The pushforward measure can also be characterized by

$$\int_{\mathcal{M}} f(T(x))d\mu(x) = \int_{T(\mathcal{M})} f(y)dT_{\#}\mu(y),$$

for all continuous functions $f : \mathbb{R}^d \rightarrow \mathbb{R}$. We assume that T is a diffeomorphism between \mathcal{M} and $\text{supp}(T_{\#}\mu)$, meaning that T is bijective, smooth, and its inverse is smooth. Therefore, the pushforward measure $T_{\#}\mu$ is absolutely continuous with respect to the Lebesgue measure on \mathbb{R}^d , and there exists a density function ρ_T such that $dT_{\#}\mu(x) = \rho_T(x)dx$.

3 Geometry-Preserving Encoder/Decoder (GPE)

We first propose a geometry-preserving encoder, where “geometry-preserving” refers to a concept introduced in (Lee et al., 2023; Yang et al., 2024). We call an encoder α -geometry-preserving if it is a mapping T from \mathcal{M} to \mathbb{R}^d that is α -bi-Lipschitz, where $0 < \alpha \leq 1$. Recall that T is α -bi-Lipschitz if and only if

$$\alpha\|x - x'\| \leq \|T(x) - T(x')\| \leq \frac{1}{\alpha}\|x - x'\|, \quad \forall x, x' \in \mathcal{M}. \quad (2)$$

In practical scenarios, computing an encoder that satisfies the α -bi-Lipschitz condition for all pairs of points $(x, x') \in \mathcal{M}^2$ is challenging. Therefore, we consider a weaker version of the α -bi-Lipschitz condition.

Definition 1. We say that a map $T : \mathcal{M} \rightarrow \mathbb{R}^d$ satisfies the weak α -bi-Lipschitz condition on a subset $A \subset \mathcal{M}^2$ if

$$\alpha^2 \|x - x'\|^2 - (1 - \alpha^2) \leq \|T(x) - T(x')\|^2 \leq \frac{1}{\alpha^2} \|x - x'\|^2 + \left(\frac{1}{\alpha^2} - 1 \right),$$

for all $(x, x') \in A$.

This weak α -bi-Lipschitz property has a connection to the standard bi-Lipschitz condition under the additional assumption that we evaluate it on pairs of points that are sufficiently well-separated. We present this connection in the following proposition.

Proposition 2. Let $T : \mathcal{M} \rightarrow \mathbb{R}^d$ be a weak α -bi-Lipschitz map on a subset $A \subset \mathcal{M}^2$. Given $0 < \gamma < 1$, T satisfies the following bi-Lipschitz condition:

$$\alpha(1 - \gamma) \|x - x'\|^2 \leq \|T(x) - T(x')\|^2 \leq \left(\frac{1}{\alpha} + \gamma \right) \|x - x'\|^2, \quad \forall (x, x') \in \tilde{A},$$

where \tilde{A} is a subset of A defined as

$$\tilde{A} := \left\{ (x, x') \in A : \|x - x'\|^2 \geq \frac{1 - \alpha}{\alpha\gamma} \right\}.$$

In simple language, the above proposition shows that the weak bi-Lipschitz condition implies the regular bi-Lipschitz condition for sufficiently separated pairs of points.

Next, we discuss how to compute a weak α -bi-Lipschitz encoder. Before we introduce our framework, we first review the Gromov-Monge embedding (GME) cost function introduced in Lee et al. (2023); Yang et al. (2024):

$$C_{\text{GME}}(T, \mu) := \mathbb{E}_{(x, x') \sim \mu^2} \left(c_X(x, x') - c_Y(T(x), T(x')) \right)^2,$$

where $c_X : \mathcal{M} \times \mathcal{M} \rightarrow \mathbb{R}$ and $c_Y : \mathbb{R}^d \times \mathbb{R}^d \rightarrow \mathbb{R}$ are cost functions defined in the data space and the latent space, respectively. Throughout this paper, we fix

$$c_X(x, x') = \log(1 + \|x - x'\|^2) \quad \text{and} \quad c_Y(y, y') = \log(1 + \|y - y'\|^2).$$

Thus, the GME cost function we consider takes the form

$$C_{\text{GME}}(T, \mu) := \mathbb{E}_{(x, x') \sim \mu^2} \left[\log \left(\frac{1 + \|T(x) - T(x')\|^2}{1 + \|x - x'\|^2} \right)^2 \right]. \quad (3)$$

In Lee et al. (2023), it is shown that with this particular choice of cost functions, if T satisfies a small value of the GME cost, then it follows that T satisfies the weak α -bi-Lipschitz condition for the majority of pairs of points in \mathcal{M}^2 . We review this result in the following theorem.

Theorem 3 (Lee et al. (2023)). Fix $0 < \alpha \leq 1$ and $\varepsilon_{\text{GME}} \geq 0$. Given a distribution $\mu \in \mathbb{P}(\mathcal{M})$, suppose $T : \mathcal{M} \rightarrow \mathbb{R}^d$ satisfies $C_{\text{GME}}(T, \mu) \leq \varepsilon_{\text{GME}}$. Then, T satisfies the weak α -bi-Lipschitz condition on a subset $A \subset \mathcal{M}^2$ where A satisfies

$$\mu^2(A) > 1 - \frac{\varepsilon_{\text{GME}}}{4(\log \alpha)^2}.$$

We are now ready to present the geometry-preserving encoder/decoder (GPE) framework:

GPE Framework Given an empirical distribution $\hat{\mu}_n = \frac{1}{n} \sum_{i=1}^n \delta_{x_i}$, where $\{x_i\}$ are sampled from the data distribution $\mu \in \mathbb{P}(\mathcal{M})$:

1. Compute the GPE encoder by solving the following minimization problem:

$$\inf_{T: \mathcal{M} \rightarrow \mathbb{R}^d} C_{\text{GME}}(T, \hat{\mu}_n). \quad (4)$$

2. Once the GPE encoder is computed, calculate the GPE decoder by solving:

$$\min_{S: \mathbb{R}^d \rightarrow \mathcal{M}} \mathbb{E}_{x \sim \hat{\mu}_n} L_{\text{rec}}(S \circ T(x), x)$$

where L_{rec} is a quadratic cost function defined as

$$L_{\text{rec}}(S \circ T(x), x) = \|S \circ T(x) - x\|^2.$$

Note that there are several differences in the usage of the GME cost between this paper and the works by Lee et al. (2023) and Yang et al. (2024). The key distinction is that the cost function in (3) was used as a regularization term in a minimax problem within the GAN framework and hyperbolic neural networks to weakly enforce the geometry-preserving property on the encoder. However, in this paper, we use the GME cost as the sole minimization objective, making it crucial to achieve the smallest possible value, which implies the weak bi-Lipschitz condition on a large subset of the domain \mathcal{M}^2 . This approach necessitates the development of a more refined theory for this variational formulation to establish stability and convergence results for the GME cost. We also discuss Hessian analysis to explore the smoothness properties and convergence results of the gradient descent algorithm applied to the GME cost. Additionally, given an encoder that minimizes the GME cost, we present new theorems for error bounds, demonstrating that this theory can be both useful and practical in the latent diffusion model when using the GPE framework.

Remark 4. *The main objective of the encoder loss in eq. (3) is to find an embedding map close to a 1-bi-Lipschitz map. This objective is essentially the same as that of Multidimensional Scaling (MDS) (Carroll and Arabie, 1998). However, MDS requires the entire dataset to compute the embedding map, which may not even be feasible for very large datasets, such as those considered in the numerical experiments in Section 7 (e.g., CIFAR-10 and CelebA). In contrast, the approach proposed in this paper, based on the GME cost using neural networks, allows for minibatch training, making it more suitable for large datasets.*

3.1 Comparing GPE with VAE

The GPE framework differs from the VAE framework in its approach and objectives. In the VAE framework, the primary goal is to embed the data distribution onto a d -dimensional standard normal distribution \mathcal{N} in the latent space. Specifically, it seeks an encoder $T: \mathcal{M} \rightarrow \mathbb{R}^d$ and a decoder $S: \mathbb{R}^d \rightarrow \mathcal{M}$ that satisfy:

$$T_{\#}\mu = \mathcal{N} \quad \text{and} \quad S = T^{-1}. \quad (5)$$

To achieve this, the VAE framework employs the Evidence Lower Bound (ELBO) cost, formulated as:

$$\min_{\substack{T:\mathcal{M}\rightarrow\mathbb{R}^d \\ S:\mathbb{R}^d\rightarrow\mathcal{M}}} \left\{ L_{\text{ELBO}}(T, S) = L_{\text{rec}}(S, T) + \lambda L_{\text{prior}}(T_{\#}\mu, \mathcal{N}) \right\},$$

where L_{rec} is a reconstruction cost minimized when $S = T^{-1}$, and L_{prior} is a prior constraint term (often chosen to be Kullback-Leibler divergence) to enforce the pushforward relation in (5). The parameter λ balances the trade-off between these two terms. However, selecting λ is challenging, and different choices can yield significantly different results, making VAE training difficult. The encoder satisfying (5) is by no means geometry-preserving, as it does not satisfy the α -bi-Lipschitz condition with α close to 1. For example, when considering the data distribution of Gaussian mixtures, the encoder T must map this mixture of Gaussians to a single Gaussian. Inevitably, there are pairs of points where it almost collapses, causing α to approach 0. Figure 1 provides an example illustrating this behavior.

In contrast, the GPE framework allows for independent training of the encoder and decoder through:

$$\inf_{T:\mathcal{M}\rightarrow\mathbb{R}^d} C_{\text{GME}}(T, \mu), \quad \min_{S:\mathbb{R}^d\rightarrow\mathcal{M}} L_{\text{rec}}(S, T).$$

This independence simplifies the training process, eliminating the need to balance or trade off parameters. Each minimization problem can be analyzed separately, with both demonstrating stable and efficient training properties. Additionally, by Theorem 3, minimizing the GME cost ensures that T satisfies the weak α -bi-Lipschitz condition, which also implies the regular bi-Lipschitz condition for well-separated pairs of points. The difference between the embedded distributions from the VAE and GPE encoders is also discussed in an experiment presented by Lee et al. (2023).

In what follows, we provide theoretical properties of the GPE framework for the reconstruction task from an optimization perspective, demonstrating that the cost function (3) is ε -convex, where ε is the value of the cost function $\varepsilon = C_{\text{GME}}(T, \mu)$. Thus, as the cost value becomes smaller, the problem becomes more convex. Furthermore, we show that computing the decoder can become more efficient and faster if the encoder adheres to the α -geometry-preserving structure with α close to 1. Lastly, we establish an error bound for the GPE framework applied to generation tasks.

4 Theoretical properties of GPE

In this section, we focus on the efficiency of training the GPE encoder and decoder, as well as the convergence analysis of using gradient descent algorithms for this purpose. To achieve this, we provide theoretical results that include a Hessian analysis of the minimization problem for the GPE encoder in (3) (Section 4.1) and for the decoder given the α -geometry-preserving encoder (Section 4.2). Throughout the theoretical results presented in Section 4 and Section 5, we assume a minimal regularity condition on the GPE encoders T .

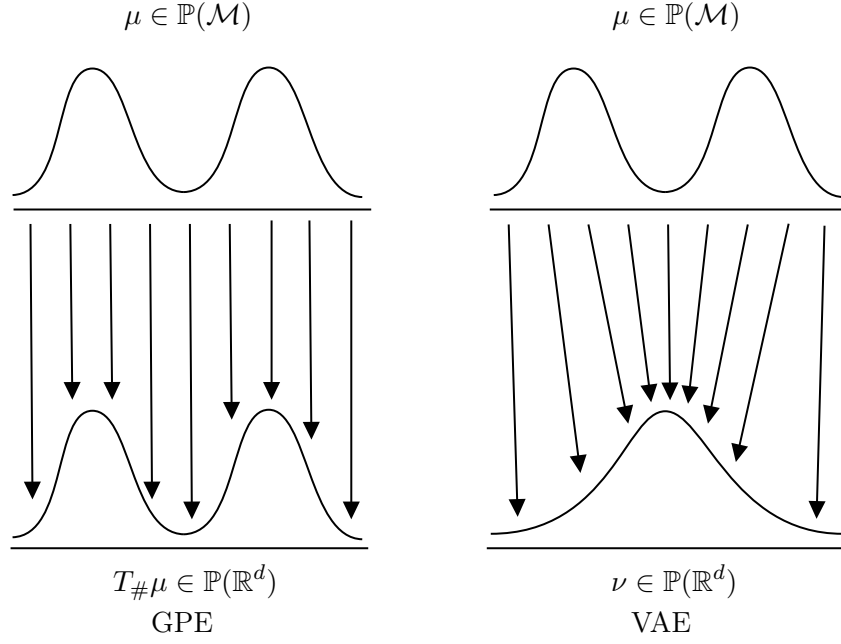


Figure 1: Illustration showing how GPE (left) and VAE (right) encoders work. The GPE encoder embeds the data distribution into the latent space while maintaining the geometric structure of the data distribution. In contrast, the VAE encoder maps the data distribution onto the latent distribution (or a prior distribution) ν such that $T_{\#}\mu \approx \nu$.

Minimal Regularity Assumption on GPE Encoders:

$$\mathcal{T}_\beta := \left\{ T : \mathcal{M} \rightarrow \mathbb{R}^d : \begin{array}{l} T \text{ is invertible, } T(x) = 0 \text{ for some } x \in \mathcal{M}, \text{ and} \\ \|T(x) - T(x')\| \leq \beta \|x - x'\|, \forall x, x' \in \mathcal{M} \end{array} \right\}. \quad (6)$$

The constant β may be very large, depending on how the encoder T is defined or parameterized. Thus, the set \mathcal{T}_β represents the minimal regularity required of the encoder for the validity of the subsequent theoretical results. The first immediate property arising from this regularity assumption is as follows:

Proposition 5. *Fix $\beta > 0$ and let $T \in \mathcal{T}_\beta$. Then, the GME cost in (3) is bounded above and below such that*

$$0 \leq C_{\text{GME}}(T, \mu) \leq (\log(\max(\beta^2, 1 + \text{diam}(\mathcal{M})^2)))^2$$

for any $\mu \in \mathbb{P}(\mathcal{M})$. Furthermore, there exists a minimizer T^* such that

$$C_{\text{GME}}(T^*, \mu) = \min_{T \in \mathcal{T}_\beta} C_{\text{GME}}(T, \mu).$$

Remark 6. *Note that Proposition 5 shows that the cost function attains a minimizer. Thus, the problem in eq. (4) within the constraint \mathcal{T}_β becomes a min problem instead of an inf problem.*

Proof From the definitions of C_{GME} from eq. (3) and constraint \mathcal{T}_β in eq. (6),

$$\begin{aligned} C_{\text{GME}}(T, \mu) &= \mathbb{E}_{(x, x') \sim \mu^2} \left[\log \left(\frac{1 + \|T(x) - T(x')\|^2}{1 + \|x - x'\|^2} \right)^2 \right] \\ &\leq \mathbb{E}_{(x, x') \sim \mu^2} \left[\log \left(\max \left(\frac{1 + \beta^2 \|x - x'\|^2}{1 + \|x - x'\|^2}, 1 + \|x - x'\|^2 \right) \right)^2 \right] \\ &\leq \log \left(\max(\beta^2, 1 + \text{diam}(\mathcal{M})^2) \right)^2. \end{aligned}$$

The second part of the proposition follows from the facts that C_{GME} is a continuous function with respect to T and that the constraint set \mathcal{T}_β is compact. \blacksquare

From this point onward, we will define a positive constant B as

$$B := \log \left(\max(\beta^2, 1 + \text{diam}(\mathcal{M})^2) \right), \quad (7)$$

since it frequently appears in the subsequent theoretical results.

4.1 Stability of GPE encoder training

In this section, we present a theorem that establishes an approximate convexity property of the GME cost when $C_{\text{GME}}(T, \mu)$ is sufficiently small. First, let us review the notion of first and second variations that will be used throughout the paper.

Definition 7. Given a Hilbert space \mathcal{H} and a function $f : \mathcal{H} \rightarrow \mathbb{R}$, the first variation of a functional f at $u \in \mathcal{H}$ in the direction of $h \in \mathcal{H}$ is defined by

$$\delta f(u)(h) = \lim_{t \rightarrow 0} \frac{f(u + th) - f(u)}{t}. \quad (8)$$

The second variation of f at u in the direction of h is defined by

$$\delta^2 f(u)(h, h) = \lim_{t \rightarrow 0} \frac{\delta f(u + th)(h) - \delta f(u)(h)}{t} \quad (9)$$

Using this definition, we find the explicit formula for the second variation of the GME cost. The derivation of the second variation is based on straightforward algebraic computations. The proof of Proposition 8 is provided in the appendix.

Proposition 8. Given a distribution $\mu \in \mathbb{P}(\mathcal{M})$ and maps $T, h : \mathcal{M} \rightarrow \mathbb{R}^d$ and $T, h \in L^4(\mathcal{M})$, the first and the second variations of the GME cost at T in the direction of h take the following forms:

$$\begin{aligned} \delta C_{\text{GME}}(T, \mu)(h) &= \int_{\mathcal{M}^2} 4 \log \left(\frac{\|T_{x, x'}\|^2 + 1}{\|x - x'\|^2 + 1} \right) \frac{\langle T_{x, x'}, h_{x, x'} \rangle}{\|T_{x, x'}\|^2 + 1} d\mu d\mu, \\ \delta^2 C_{\text{GME}}(T, \mu)(h, h) &= \int_{\mathcal{M}^2} 4 \log \left(\frac{\|T_{x, x'}\|^2 + 1}{\|x - x'\|^2 + 1} \right) \left(\frac{\|h_{x, x'}\|^2}{\|T_{x, x'}\|^2 + 1} - 2 \left(\frac{\langle T_{x, x'}, h_{x, x'} \rangle}{\|T_{x, x'}\|^2 + 1} \right)^2 \right) \\ &\quad + 8 \left(\frac{\langle T_{x, x'}, h_{x, x'} \rangle}{\|T_{x, x'}\|^2 + 1} \right)^2 d\mu d\mu. \end{aligned}$$

Here, for any function $f : \mathcal{M} \rightarrow \mathbb{R}^d$, we denote $f_{x, x'} = f(x) - f(x')$ for simplicity.

The following theorem demonstrates the convexity of the GME cost function. Although the cost function is inherently nonconvex, the theorem indicates that as the optimization process progresses and the GME cost function decreases, the cost function becomes less nonconvex.

Theorem 9. *Fix $\varepsilon > 0$ and $\beta > 0$. If $T \in \mathcal{T}_\beta$, and $C_{\text{GME}}(T, \mu) < \varepsilon$, then the Hessian of the GME cost is bounded as follows:*

$$-16\sqrt{\varepsilon}\|h\|_{L^4(\mathcal{M})}^2 < \delta^2 C_{\text{GME}}(T, \mu)(h, h) < 8(2B + 1)\|h\|_{L^2(\mathcal{M})}^2, \quad (10)$$

for all $h : \mathcal{M} \rightarrow \mathbb{R}^d$ and $h \in L^4(\mathcal{M})$ where B is defined in (7).

Proof For simplicity, we use throughout the proof, the notation $f_{x,x'} := f(x) - f(x')$ for any $f : \mathcal{M} \rightarrow \mathbb{R}^d$. From Proposition 8, the second variation of the GME cost implies that for $T, h : \mathcal{M} \rightarrow \mathbb{R}^d$

$$\begin{aligned} & \frac{1}{4}\delta^2 C_{\text{GME}}(T, \mu)(h, h) \\ &= \int_{\mathcal{M}^2} \log\left(\frac{\|T_{x,x'}\|^2 + 1}{\|x - x'\|^2 + 1}\right) \left(\frac{\|h_{x,x'}\|^2}{\|T_{x,x'}\|^2 + 1} - 2\left(\frac{\langle T_{x,x'}, h_{x,x'} \rangle}{\|T_{x,x'}\|^2 + 1}\right)^2\right) \\ & \quad + 2\left(\frac{\langle T_{x,x'}, h_{x,x'} \rangle}{\|T_{x,x'}\|^2 + 1}\right)^2 d\mu d\mu \end{aligned} \quad (11)$$

$$\geq - (C_{\text{GME}}(T, \mu))^{1/2} \left(\int_{\mathcal{M}^2} \left(\frac{\|h_{x,x'}\|^2}{\|T_{x,x'}\|^2 + 1} - 2\left(\frac{\langle T_{x,x'}, h_{x,x'} \rangle}{\|T_{x,x'}\|^2 + 1}\right)^2 \right)^2 d\mu d\mu \right)^{1/2} \quad (12)$$

where we used Hölder's inequality in the last line. Note that from the last line, the following holds:

$$0 \leq \frac{\|h_{x,x'}\|^2}{\|T_{x,x'}\|^2 + 1} \leq \|h_{x,x'}\|^2$$

and using Cauchy-Schwarz inequality and $t/(t+1)^2 \leq 1/2$ for $t \geq 0$:

$$0 \leq \left(\frac{\langle T_{x,x'}, h_{x,x'} \rangle}{\|T_{x,x'}\|^2 + 1}\right)^2 \leq \frac{\|T_{x,x'}\|^2 \|h_{x,x'}\|^2}{(\|T_{x,x'}\|^2 + 1)^2} \leq \frac{\|h_{x,x'}\|^2}{4}. \quad (13)$$

Combining these two inequalities we have

$$\left| \frac{\|h_{x,x'}\|^2}{\|T_{x,x'}\|^2 + 1} - 2\left(\frac{\langle T_{x,x'}, h_{x,x'} \rangle}{\|T_{x,x'}\|^2 + 1}\right)^2 \right| \leq \|h_{x,x'}\|^2. \quad (14)$$

Furthermore, note that by using the inequality $(a+b)^p \leq 2^{p-1}(a^p + b^p)$ for $a, b \geq 0$ and $p \geq 1$, we can bound $\int_{\mathcal{M}^2} \|h_{x,x'}\|^p d\mu d\mu$ by

$$\int_{\mathcal{M}^2} \|h_{x,x'}\|^p d\mu d\mu \leq \int_{\mathcal{M}^2} 2^{p-1}(\|h(x)\|^p + \|h(x')\|^p) d\mu d\mu \leq 2^p \int_{\mathcal{M}} \|h(x)\|^p d\mu. \quad (15)$$

Using the above inequalities and $C_{\text{GME}}(T, \mu) < \varepsilon$, we bound the right-hand side of (12) below by

$$-4\sqrt{\varepsilon} \left(\int_{\mathcal{M}^2} \|h_{x,x'}\|^4 d\mu d\mu \right)^{1/2}.$$

Now, let us find the upper bound of the hessian. Since $T \in \mathcal{T}_\beta$, we have the following bound:

$$\left| \log \left(\frac{\|T_{x,x'}\|^2 + 1}{\|x - x'\|^2 + 1} \right) \right| \leq \log(\max(\beta^2, 1 + \text{diam}(\mathcal{M}^2))) =: B, \quad (16)$$

for all $(x, x') \in \mathcal{M}^2$. From (11), using (13), (14), (15), and (16), we can bound the hessian above by

$$B \int_{\mathcal{M}^2} \|h_{x,x'}\|^2 d\mu d\mu + \frac{1}{2} \int_{\mathcal{M}^2} \|h_{x,x'}\|^2 d\mu d\mu \leq 2(2B + 1) \|h\|_{L^2(\mathcal{M})}^2.$$

This completes the proof. ■

Theorem 9 shows that as the cost function decreases, the minimization problem becomes more stable because the lower bound of the Hessian approaches 0, indicating that the cost function exhibits more convex behavior. Additionally, the upper bound of the Hessian suggests that the GME cost function is smooth, which is crucial for the convergence of the gradient descent algorithm when applied to a nonconvex function. In the next corollary which is a direct consequence from Theorem 9, we present our convergence analysis of gradient descent on the GME cost.

Corollary 10. *Given a data distribution $\mu \in \mathbb{P}(\mathcal{M})$ and a latent space \mathbb{R}^d , let $\delta \geq 0$ be the minimal value of $C_{\text{GME}}(T, \mu)$ such that*

$$\delta \leq C_{\text{GME}}(T, \mu), \quad \forall T : \mathcal{M} \rightarrow \mathbb{R}^d.$$

Let $T^{(k)}$ be a sequence of maps generated by the following gradient descent steps:

$$T^{(k+1)} = T^{(k)} - \sigma \nabla C_{\text{GME}}(T^{(k)}, \mu), \quad k \geq 0 \quad (17)$$

with $T^{(0)}$ as the initial point. Here, ∇C_{GME} is a gradient of C_{GME} with respect to T . With the choice of $\sigma = 1/(8(2B + 1))$, the gradient descent will find a $T^{(k)}$ that is an almost stationary point in a finite number of steps such that

$$\min_{k < K} \|\nabla_{L^2} C_{\text{GME}}(T^{(k)}, \mu)\|^2 \leq \frac{16}{K} (2B + 1) (C_{\text{GME}}(T^{(0)}, \mu) - \delta),$$

where B is defined in (7).

Corollary 10 shows the gradient descent algorithm for T and its convergence rate. In practice, the function T is approximated using a neural network architecture. This network is parameterized by a set of learnable parameters, which are optimized during training. Thus, gradient descent operates on these neural network parameters rather than directly on

the training data $x \sim \mu$. By setting θ as a vector of neural network parameters and $T = T_\theta$ as the neural network function approximating T , the gradient descent algorithm takes the form:

$$\theta^{(k+1)} = \theta^{(k)} - \sigma \nabla_{\theta} C_{\text{GME}}(T_{\theta^{(k)}}, \mu)$$

where ∇_{θ} is a gradient with respect to θ . However, as shown in Jacot et al. (2018), it is well known that neural network optimization can be understood as a gradient descent formulation similar to eq. (17), except that it includes an additional preconditioning operator based solely on the neural network architecture. Thus, gradient descent takes the form:

$$T_{\theta^{(k+1)}} = T_{\theta^{(k)}} - \sigma K^{(k)} \nabla C_{\text{GME}}(T_{\theta^{(k)}}, \mu),$$

where $K^{(k)}$ is the preconditioning operator at iteration step (k) . This preconditioning operator affects the training dynamics, making it different from standard gradient descent as in eq. (17). We will not delve further into this here, but it is an interesting direction for future research, as it could explain why, in practice, one consistently obtains solutions for T with sufficiently small values of C_{GME} using neural network optimization, rather than converging to the local minimizer with a large C_{GME} value.

4.2 Efficiency of decoder training given a bi-Lipschitz encoder

The primary advantage of using an α -bi-Lipschitz encoder with α close to 1 is that it can lead to more efficient computation of the decoder that minimizes the reconstruction cost. Consider the following reconstruction cost function given an encoder T :

$$L_{\text{rec}}(S, \mu) := \mathbb{E}_{x \sim \mu} [c(S \circ T(x), x)] \tag{18}$$

where c is a convex function that is minimized when $S \circ T(x) = x$. The subsequent theorem, which provides upper and lower bounds on the Hessian of the reconstruction cost, highlights the theoretical benefits of having an α -geometry-preserving property in the encoder.

Theorem 11. *Given a data distribution $\mu \in \mathbb{P}(\mathcal{M})$ and an α -bi-Lipschitz map $T : \mathcal{M} \rightarrow \mathbb{R}^d$, consider the reconstruction cost in (18), where $c : \mathcal{M} \times \mathcal{M} \rightarrow \mathbb{R}$ is a convex function such that $c(x, y) \geq 0$ for all $x, y \in \mathcal{M}$, and $c(x, y) = 0$ if and only if $x = y$. Assume the second derivatives of c are bounded as follows:*

$$c_{\min} I \leq \nabla_{xx}^2 c = \nabla_{yy}^2 c \leq c_{\max} I$$

for some constants $0 < c_{\min} \leq c_{\max}$.

The second variation of the cost function satisfies

$$\alpha^d c_{\min} \rho_{\min} \|h\|_{L^2(\mathbb{R}^d)}^2 \leq \delta^2 L_{\text{rec}}(S, \mu)(h, h) \leq \frac{c_{\max} \rho_{\max}}{\alpha^d} \|h\|_{L^2(\mathbb{R}^d)}^2. \tag{19}$$

Thus, the map S satisfying $S(T(x)) = x$ for all $x \in \mathcal{M}$ is the unique solution of the problem.

Proof For a test function $h : \mathbb{R}^d \rightarrow \mathcal{M}$, the Euler-Lagrange equation takes the form

$$\mathbb{E}_{x \sim \mu} [(h(T(x)), \partial_x c(S(T(x)), x))] = 0.$$

It follows that the map S satisfying $S(T(x)) = x$ for all $x \sim \mu$ satisfies the equation thus is a minimizer.

Using the formulation of the second variation of the cost function in Proposition 8 and the fact that $T_{\#}\mu$ is absolutely continuous, we have

$$\begin{aligned}
 & \delta^2 L_{\text{rec}}(S, \mu)(h, h) \\
 &= \mathbb{E}_{x \sim \mu} [\langle h(T(x)), \nabla_{xx}^2 c(S(T(x)), x) h(T(x)) \rangle] \\
 &= \int_{\mathbb{R}^d} [\langle h(y), \nabla_{xx}^2 c(S(y), T^{-1}(y)) h(y) \rangle] dT_{\#}\mu(y) \\
 &= \int_{\mathbb{R}^d} [\langle h(y), \nabla_{xx}^2 c(S(y), T^{-1}(y)) h(y) \rangle] \rho_T(y) dy \\
 &= \int_{\mathbb{R}^d} [\langle h(y), \nabla_{xx}^2 c(S(y), T^{-1}(y)) h(y) \rangle] \frac{\rho(T^{-1}(y))}{|\det(\nabla T(T^{-1}(y)) \nabla T(T^{-1}(y))^T)|^{1/2}} dy \\
 &\geq \alpha^d c_{\min} \rho_{\min} \|h\|_{L^2(\mathbb{R}^d)}^2.
 \end{aligned}$$

Similarly, the other direction of the inequality can be shown.

$$\delta^2 L_{\text{rec}}(S)(h, h) \leq \frac{c_{\max} \rho_{\max}}{\alpha^d} \|h\|_{L^2(\mathbb{R}^d)}^2.$$

Since the function is a strongly convex function, the function admits a unique solution described above. \blacksquare

According to Theorem 11, the upper and lower bounds of the Hessian of the cost function in (19) are influenced by α , which shows that the Hessian has a tighter bound when given an encoder with α -geometry-preserving properties with α closer to 1.

The following theorem shows the convergence rate of the gradient descent algorithm on the reconstruction cost with respect to the α -geometry-preserving parameter α . The proof is provided in the appendix.

Theorem 12. *Consider a step size $\sigma > 0$ and a sequence $S^{(k)}$ that follows a gradient descent algorithm on (18), starting from an initial point $S^{(0)}$, such that for $k = 0, 1, 2, \dots$,*

$$S^{(k+1)} = S^{(k)} - \sigma \nabla L_{\text{rec}}(S^{(k)}, \mu).$$

Choose $\sigma = \frac{\alpha^d}{c_{\max} \rho_{\max}}$. Then,

$$\|S^{(k)} - S^{(*)}\| \leq \left(1 - \frac{\alpha^{2d} c_{\min} \rho_{\min}}{c_{\max} \rho_{\max}}\right)^k \|S^{(0)} - S^{(*)}\|.$$

As the encoder better satisfies the α -geometry-preserving property with α closer to 1, the optimization process for computing the decoder map S becomes more efficient and accelerated.

Note that Theorem 11 and Theorem 12 are predicated on the assumption that T is α -bi-Lipschitz. This assumption is crucial for the proof, as it permits the bounding of $\|\nabla T\|$. However, under a weak α -bi-Lipschitz condition, one cannot assume the existence

of a positive constant $0 < c \leq 1$ such that $c < \|T(x) - T(x')\|/\|x - x'\| < 1/c$ for any arbitrarily close pair of points $(x, x') \in \mathcal{M}^2$. Although the theorems rely on the α -bi-Lipschitz assumption, numerical results show that a weak α -bi-Lipschitz condition on the encoder is sufficient to accelerate decoder training. The training efficiency of the decoder improves as the encoder achieves a smaller GME cost, which corresponds to a larger subset of the domain where the weak α -bi-Lipschitz condition holds with α close to 1.

5 Efficiency of GPE in LGM

In this section, we provide error bounds to demonstrate that the generated distribution from the GPE framework can efficiently approximate the input data distribution. Let us briefly review how the latent generative model (LGM) works. Suppose we have the input data distribution $\mu \in \mathbb{P}(\mathcal{M})$ and a latent distribution $\nu \in \mathbb{P}(\mathbb{R}^d)$. In the latent diffusion model, the generative map from ν to μ is found by considering the embedding of μ into the latent space \mathbb{R}^d with an encoder $T : \mathcal{M} \rightarrow \mathbb{R}^d$ and computing a flow map $R : \mathbb{R}^d \rightarrow \mathbb{R}^d$ that generates trajectories from samples in ν to the embedded distribution $T_{\#}\mu$, such that $R_{\#}\nu = T_{\#}\mu$. This flow map is computed by training diffusion models, such as score-based generative models (Song et al., 2020) and conditional flow matching models (Lipman et al., 2022). Thus, the generated distribution can be described by a composite map $G = S \circ R$, where $S : \mathbb{R}^d \rightarrow \mathcal{M}$ is a decoder such that $S = T^{-1}$. See Figure 2 for the visualization of LGM framework.

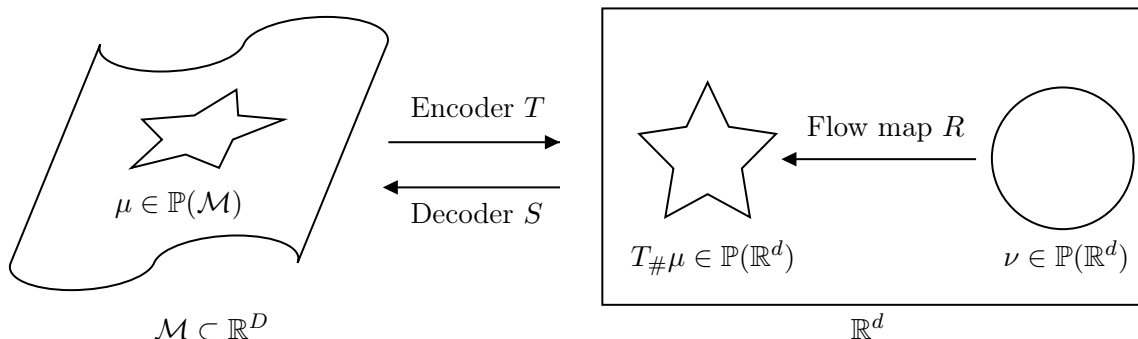


Figure 2: Visualization of latent generative model framework

This section presents two main theorems. The first theorem, Theorem 13, establishes that if the encoder is α -geometry-preserving, the error bound between the data distribution and the generated distribution (from the latent distribution) is determined by three key factors:

- (i) The parameter α ,
- (ii) The reconstruction loss, and
- (iii) The Wasserstein distance $W_p(T_{\#}\mu, R_{\#}\nu)$ between the embedded data distribution $T_{\#}\mu$ and the pushforward measure $R_{\#}\nu$ of the latent distribution, which is computed using the flow map from the diffusion models.

The theorem shows that the error bound approaches 0 as the number of points in the dataset increases and the rate improves as α is closer to 1. The second theorem, Theorem 14, is similar to Theorem 13, but the assumption changes to T being a minimizer of the GME cost rather than an α -bi-Lipschitz function. This shows that by minimizing the GME cost, one can achieve a tight error bound for LGM. The proofs of two theorems are presented in Section 5.1 and Section 5.2.

Theorem 13 (Error bound of α -bi-Lipschitz encoder in LGM). *Fix $0 < \alpha \leq 1$, $\varepsilon > 0$, $\varepsilon_{\text{dif}}, \varepsilon_{\text{rec}} > 0$ and $1 \leq p \leq p'$. Let $\mu \in \mathbb{P}(\mathcal{M})$ and $\nu \in \mathbb{P}(\mathbb{R}^d)$, $\hat{\mu}_n = \frac{1}{n} \sum_{i=1}^n \delta_{x_i}$ be an empirical distribution where x_i are sampled from μ , and let $T : \mathcal{M} \rightarrow \mathbb{R}^d$ be an α -bi-Lipschitz map and $R : \mathbb{R}^d \rightarrow \mathbb{R}^d$ be a flow map such that $R_{\#}\nu$ is an absolutely continuous measure satisfying*

$$dR_{\#}\nu(x) = \rho_R(x)dx, \quad \sup_{x \in \mathbb{R}^d} \rho_R(x) \leq (R_{\#}\nu)_{\max} \quad (20)$$

for some nonnegative function ρ_R and a positive constant $(R_{\#}\nu)_{\max} > 0$ and

$$W_p(T_{\#}\hat{\mu}_n, R_{\#}\nu) < \varepsilon_{\text{dif}}. \quad (21)$$

Let $S : \mathbb{R}^d \rightarrow \mathcal{M}$ be a decoder satisfying

$$L_{\text{rec}}(S, \hat{\mu}_n) < \varepsilon_{\text{rec}} \quad (22)$$

where L_{rec} is defined in (18) with $c(x, x') = \|x - x'\|^{p'}$. Denote by $\Omega_d := \text{supp}(R_{\#}\nu)$. Then, there exist positive constants $C_1 = C_1(p, p', \text{diam}(\mathcal{M}), (R_{\#}\nu)_{\max}, \rho_{\min})$ and $C_2 = C_2(T_{\#}\mu, d)$ such that the event

$$\begin{aligned} & W_p(\mu, (S \circ R)_{\#}\nu) \\ & \leq 2 \left(\frac{C_1}{\alpha^{d/p}} (\varepsilon_{\text{rec}} + \varepsilon)^{1/p} + \frac{1}{\alpha} (\varepsilon_{\text{dif}} + C_2 n^{-2/(d+4)}) + \text{diam}(\mathcal{M}) (R_{\#}\nu(\Omega_d \setminus T(\mathcal{M})))^{1/p} \right) \end{aligned}$$

holds with probability at least $1 - 2 \exp\left(-\frac{n\varepsilon}{6(1+\varepsilon/3)}\right)$. Here, W_p is the Wasserstein- p distance.

Note that the error bound in Theorem 13 depends on the latent dimension d , which is much smaller than the data distribution dimension D . This is due to the encoder, which converts the comparison of two D -dimensional distributions to the comparison of two d -dimensional ones, allowing a more efficient bound with respect to dimensionality. Furthermore, the α -geometry-preserving constant α directly affects the upper bound of the Wasserstein distance between the data distribution and the generated distribution. The bound becomes tighter as α approaches 1. Thus, having α close to 1 allows the generative map more room for error in approximating the embedded distribution in the latent space, making the computation more efficient in the LGM framework. Therefore, the theorem highlights the importance of an encoder with α -geometry-preserving with α closer to 1 for better performance in LGM.

Theorem 13 is based on the assumption that the encoder T exhibits the α -bi-Lipschitz property with α close to 1 for all pairs of points in \mathcal{M} . Thus, in the next theorem, we present an upper bound on the performance of the GPE-based LGM with respect to the encoder T that minimizes the GME cost. The theorem provides the bound as the Wasserstein distance

between the data distribution and the generated distribution, expressed as functions of the GME cost, the reconstruction cost, and the Wasserstein distance between $T_{\#}\mu$ (the embedded distribution) and $R_{\#}\nu$ (the pushforward distribution from the latent distribution through the flow map R). This statement holds true with high probability, given a small GME cost for the encoder. The proof is presented in Section 5.2.

Theorem 14 (Performance bound of GPE-based LGM). *Fix $\beta, \varepsilon > 0$, $\varepsilon_{\text{GME}}, \varepsilon_{\text{dif}}, \varepsilon_{\text{rec}} \geq 0$, $0 < \alpha \leq 1$, and $p \geq 1$. Given the same assumptions and conditions on $\mu, \nu, \hat{\mu}_n, R$, and S as in Theorem 13, let $T \in \mathcal{T}_\beta$ and $\hat{C}_{\text{GME}}(T, \hat{\mu}_n) \leq \varepsilon_{\text{GME}}$, where the discrete GME cost $\hat{C}_{\text{GME}}(T, \hat{\mu}_n)$ is defined in Definition 17, and B is defined in (7).*

Then there exist positive constants $C_1 = C_1(\text{diam}(\mathcal{M}), \rho_{\min}, \rho_{\max}, (R_{\#}\nu)_{\max})$, and $C_2 = C_2(T_{\#}\mu, d)$ such that the event

$$W_1(\mu, (S \circ R)_{\#}\nu) \leq C_1 \beta^d \left(\frac{\varepsilon_{\text{GME}} + B^2 \varepsilon}{(\log \alpha)^2} + \varepsilon_{\text{rec}} + \varepsilon \right) + \frac{1}{\alpha} \left(\varepsilon_{\text{dif}} + C_2 n^{-2/(d+4)} + 2(1-\alpha^2)^{1/2} \right) + \text{diam}(\mathcal{M}) R_{\#}\nu(\Omega_d \setminus T(\mathcal{M}))$$

holds with probability at least $1 - 4 \exp\left(-\frac{n\varepsilon^2}{6(1+\varepsilon/3)}\right)$.

5.1 Proof of Theorem 13

First, let us examine several lemmas related to the bounds of the reconstruction loss that will be used in proving the theorem.

Lemma 15. *Suppose $\mu \in \mathbb{P}(\mathcal{M})$ is an absolutely continuous measure satisfying (1) and $\nu \in \mathbb{P}(\mathbb{R}^d)$ is an absolutely continuous probability distribution in \mathbb{R}^d satisfying*

$$d\nu(y) = f(y)dy, \quad f(y) \leq \nu_{\max}$$

for some nonnegative function f and a positive constant ν_{\max} . Suppose $T : \mathcal{M} \rightarrow \mathbb{R}^d$ is invertible and satisfies

$$\|T(x) - T(x')\| \leq K\|x - x'\| \tag{23}$$

for all $x, x' \in \mathcal{M}$ for some $K > 0$. Then,

$$\|S - T^{-1}\|_{L^p(\nu, T(\mathcal{M}))}^p = \int_{T(\mathcal{M})} \|S(y) - T^{-1}(y)\|^p d\nu(y) \leq \frac{\nu_{\max} K^d}{\rho_{\min}} L_{\text{rec}}(S, \mu).$$

Proof By the assumption (23), we have

$$|\det(\nabla T(y) \nabla T(y)^T)|^{1/2} \leq K^d$$

for any $y \in \mathbb{R}^d$. Using the change of variables, we have

$$T_{\#}^{-1}\nu(x) = f(T(x)) |\det(\nabla T(x) \nabla T(x)^T)|^{1/2} \leq \nu_{\max} K^d. \tag{24}$$

Using the change of variables, the assumption (1), and (24), we have

$$\begin{aligned} \int_{T(\mathcal{M})} \|S(y) - T^{-1}(y)\|^p d\nu(y) &= \int_{\mathcal{M}} \|S(T(x)) - x\|^p dT_{\#}^{-1}\nu(x) \\ &\leq \frac{\nu_{\max} K^d}{\rho_{\min}} \int_{\mathcal{M}} \|S(T(x)) - x\|^p d\mu(x). \end{aligned}$$

This proves the lemma. ■

Lemma 16. *Fix $p \geq 1$ and $\varepsilon > 0$. Let $\mu \in \mathbb{P}(\mathcal{M})$ and $\hat{\mu}_n = \frac{1}{n} \sum_{i=1}^n \delta_{x_i}$ be an empirical distribution from μ , $T : \mathcal{M} \rightarrow \mathbb{R}^d$ be an encoder, $S : \mathbb{R}^d \rightarrow \mathcal{M}$ be a decoder, and the cost function $c(x, x') = \|x - x'\|^p$ in (18). Then, the following event*

$$|L_{\text{rec}}(S, \mu) - L_{\text{rec}}(S, \hat{\mu}_n)| \leq \varepsilon \text{diam}(\mathcal{M})^p$$

holds with probability at least $1 - 2 \exp\left(-\frac{n\varepsilon}{6(1+\varepsilon/3)}\right)$.

Proof We bound $|L_{\text{rec}}(S, \mu) - L_{\text{rec}}(S, \hat{\mu}_n)|$ by using Bernstein's inequality (Calder, 2020, Theorem 5.12). We begin by defining

$$F_n = \frac{1}{n} \sum_{i=1}^n f(x_i) \tag{25}$$

where

$$f(x_i) = \|S \circ T(x_i) - x_i\|^p$$

and we observe that $L_{\text{rec}}(T, \hat{\mu}_n) = F_n$. We also note that

$$\mathbb{E}[f(x)] = L_{\text{rec}}(S, \mu).$$

Since \mathcal{M} is compact, we have

$$b := \sup_{x \in \mathcal{M}} |f(x)| \leq \text{diam}(\mathcal{M})^p.$$

Furthermore, the variance is bounded by

$$\sigma^2 \leq \mathbb{E}[f(x)^2] = \int_{\mathcal{M}} \|S(T(x)) - x\|^{2p} d\mu(x) \leq \text{diam}(\mathcal{M})^{2p}.$$

Using Bernstein's inequality for U -statistics, we have

$$\mathbb{P}\left(|F_n - L_{\text{rec}}(S, \mu)| \geq t\right) \leq 2 \exp\left(-\frac{nt^2}{6(\sigma^2 + bt/3)}\right).$$

Choosing $t = \varepsilon \text{diam}(\mathcal{M})^p$ and using the bounds for b and σ we have

$$\mathbb{P}\left(|F_n - L_{\text{rec}}(S, \mu)| \geq \varepsilon \text{diam}(\mathcal{M})^p\right) \leq 2 \exp\left(-\frac{n\varepsilon^2}{6(1+\varepsilon/3)}\right).$$

This proves the lemma. ■

We are now ready to present the theorem demonstrating the importance of geometry-preserving encoder in latent generative models (LGM).

Proof of Theorem 13 From the definition of Wasserstein distance, we have

$$W_p^p(\hat{\mu}_n, (S \circ R)_\# \nu) = \min_{\gamma \in \Pi(\hat{\mu}_n, (S \circ R)_\# \nu)} \int_{\mathcal{M}^2} \|x - y\|^p d\gamma(x, y) \quad (26)$$

where $\Pi(\hat{\mu}_n, (S \circ R)_\# \nu)$ is a set of transport plans $\gamma \in \mathbb{P}(\mathcal{M} \times \mathcal{M})$ such that the first and second marginals of γ are $\hat{\mu}_n$ and $(S \circ R)_\# \nu$, respectively. Define a map $\tilde{S} : \mathcal{M} \rightarrow \mathbb{R}^d$ by

$$\tilde{S}(x) = \begin{cases} T^{-1}(x) & \text{if } x \in T(\mathcal{M}) \\ S(x) & \text{if } x \in \mathbb{R}^d \setminus T(\mathcal{M}). \end{cases}$$

Using the change of variables and a simple algebraic inequality $|a + b|^p \leq 2^{p-1}(|a|^p + |b|^p)$, we have

$$\begin{aligned} W_p^p(\hat{\mu}_n, (S \circ R)_\# \nu) &= \min_{\tilde{\gamma} \in \Pi(T_\# \hat{\mu}_n, R_\# \nu)} \int_{T(\mathcal{M}) \times \Omega_d} \|T^{-1}(x) - S(y)\|^p d\tilde{\gamma}(x, y) \\ &= \min_{\tilde{\gamma} \in \Pi(T_\# \hat{\mu}_n, R_\# \nu)} \int_{T(\mathcal{M}) \times \Omega_d} \|T^{-1}(x) - \tilde{S}(y) + \tilde{S}(y) - S(y)\|^p d\tilde{\gamma}(x, y) \\ &\leq 2^{p-1} \left(\min_{\tilde{\gamma} \in \Pi(T_\# \hat{\mu}_n, R_\# \nu)} \int_{T(\mathcal{M}) \times \Omega_d} \|T^{-1}(x) - \tilde{S}(y)\|^p d\tilde{\gamma}(x, y) \right. \\ &\quad \left. + \int_{\Omega_d} \|\tilde{S}(y) - S(y)\|^p dR_\# \nu(y) \right). \end{aligned} \quad (27)$$

Using Lemma 15, the assumption that T is α -bi-Lipschitz, and Hölder's inequality, the second term in the last line can be bounded above by

$$\int_{\Omega_d} \|\tilde{S}(y) - S(y)\|^p dR_\# \nu(y) \leq \int_{T(\mathcal{M})} \|T^{-1}(y) - S(y)\|^{p'} dR_\# \nu(y) \leq \frac{(R_\# \nu)_{\max}}{\rho_{\min} \alpha^d} L_{\text{rec}}(S, \mu).$$

Therefore, by using Lemma 16 and eq. (22), the following event

$$\int_{\Omega_d} \|\tilde{S}(y) - S(y)\|^{p'} dR_\# \nu(y) \leq \frac{(R_\# \nu)_{\max}}{\rho_{\min} \alpha^d} \left(\varepsilon_{\text{rec}} + \varepsilon \text{diam}(\mathcal{M})^{p'} \right) \quad (28)$$

holds with probability at least $1 - 2 \exp\left(-\frac{n\varepsilon}{6(1+\varepsilon/3)}\right)$.

From the integral in the first term, using the definition of \tilde{S} and the α -bi-Lipschitz property of T , we have

$$\begin{aligned} &\int_{T(\mathcal{M}) \times \Omega_d} \|T^{-1}(x) - \tilde{S}(y)\|^p d\tilde{\gamma}(x, y) \\ &= \int_{T(\mathcal{M})^2} \|T^{-1}(x) - T^{-1}(y)\|^p d\tilde{\gamma}(x, y) + \int_{T(\mathcal{M}) \times (\Omega_d \setminus T(\mathcal{M}))} \|T^{-1}(x) - S(y)\|^p d\tilde{\gamma}(x, y) \quad (29) \\ &= \int_{T(\mathcal{M})^2} \frac{1}{\alpha^p} \|x - y\|^p d\tilde{\gamma}(x, y) + \int_{T(\mathcal{M}) \times (\Omega_d \setminus T(\mathcal{M}))} \|T^{-1}(x) - S(y)\|^p d\tilde{\gamma}(x, y). \end{aligned}$$

The second term can be bounded above by

$$\begin{aligned}
 \int_{T(\mathcal{M}) \times (\Omega_d \setminus T(\mathcal{M}))} \|T^{-1}(x) - S(y)\|^p d\tilde{\gamma} &= \int_{\mathcal{M} \times (T^{-1}(\Omega_d \setminus T(\mathcal{M})))} \|x - S(T(y))\|^p d\gamma_0 \\
 &\leq \text{diam}(\mathcal{M})^p \int_{\mathcal{M}} \int_{T^{-1}(\Omega_d \setminus T(\mathcal{M}))} d(T^{-1} \circ R)_{\#}\nu(y) d\hat{\mu}_n(x) \\
 &= \text{diam}(\mathcal{M})^p \int_{\Omega_d \setminus T(\mathcal{M})} dR_{\#}\nu(y) \\
 &= \text{diam}(\mathcal{M})^p R_{\#}\nu(\Omega_d \setminus T(\mathcal{M}))
 \end{aligned}$$

where $\gamma_0 \in \Pi(\hat{\mu}_n, (T^{-1} \circ R)_{\#}\nu)$ in the second inequality. Thus, we have

$$\begin{aligned}
 \int_{T(\mathcal{M}) \times \Omega_d} \|T^{-1}(x) - \tilde{S}(y)\|^p d\tilde{\gamma}(x, y) \\
 \leq \frac{1}{\alpha^p} \int_{T(\mathcal{M})^2} \|x - y\|^p d\tilde{\gamma}(x, y) + \text{diam}(\mathcal{M})^p R_{\#}\nu(\Omega_d \setminus T(\mathcal{M})).
 \end{aligned}$$

By applying $\min_{\tilde{\gamma} \in \Pi(T_{\#}\hat{\mu}_n, R_{\#}\nu)}$ both sides and using (21), we have

$$\min_{\tilde{\gamma} \in \Pi(T_{\#}\hat{\mu}_n, R_{\#}\nu)} \int_{T(\mathcal{M}) \times \Omega_d} \|T^{-1}(x) - \tilde{S}(y)\|^p d\tilde{\gamma} \leq \frac{\varepsilon_{\text{dif}}^p}{\alpha^p} + \text{diam}(\mathcal{M})^p R_{\#}\nu(\Omega_d \setminus T(\mathcal{M})). \quad (30)$$

Combining (27), (28), and (30), the following event

$$\begin{aligned}
 &W_p^p(\hat{\mu}_n, (S \circ R)_{\#}\nu) \\
 &\leq 2^{p-1} \left(\frac{\varepsilon_{\text{dif}}^p}{\alpha^p} + \frac{(R_{\#}\nu)_{\max} \text{diam}(\mathcal{M})^{p'}}{\rho_{\min} \alpha^d} (\varepsilon_{\text{rec}} + \varepsilon) + \text{diam}(\mathcal{M})^p R_{\#}\nu(\Omega_d \setminus T(\mathcal{M})) \right)
 \end{aligned}$$

holds with probability at least $1 - 2 \exp\left(-\frac{n\varepsilon}{6(1+\varepsilon/3)}\right)$. Applying power $1/p$ on both sides and using the inequality $(a+b)^{1/p} \leq a^{1/p} + b^{1/p}$ for $a, b \geq 0$, we obtain

$$\begin{aligned}
 &W_p(\hat{\mu}_n, (S \circ R)_{\#}\nu) \\
 &\leq 2 \left(\frac{\varepsilon_{\text{dif}}}{\alpha} + \frac{C_1}{\alpha^{d/p}} (\varepsilon_{\text{rec}} + \varepsilon)^{1/p} + \text{diam}(\mathcal{M}) (R_{\#}\nu(\Omega_d \setminus T(\mathcal{M})))^{1/p} \right) \quad (31)
 \end{aligned}$$

where $C_1 = C_1(p, p', \text{diam}(\mathcal{M}), (R_{\#}\nu)_{\max}, \rho_{\min})$.

From the triangle inequality property of Wasserstein distance, we have

$$W_p(\mu, (S \circ R)_{\#}\nu) \leq W_p(\hat{\mu}_n, (S \circ R)_{\#}\nu) + W_p(\mu, \hat{\mu}_n). \quad (32)$$

From the second term, using the assumption that T is α -bi-Lipschitz and Proposition 1 from (Lee et al., 2023), we have

$$W_p(\mu, \hat{\mu}_n) \leq \frac{1}{\alpha} W_p(T_{\#}\mu, T_{\#}\hat{\mu}_n).$$

By applying the expectation over samples and using the result from Horowitz and Karandikar (1994), we have

$$\mathbb{E}W_p(\mu, \hat{\mu}_n) \leq \frac{1}{\alpha} \mathbb{E}W_p(T_{\#}\mu, T_{\#}\hat{\mu}_n) \leq \frac{C_2 n^{-2/(d+4)}}{\alpha} \quad (33)$$

where C_2 depends only on $T_{\#}\mu$ and d .

Combining (31), (32), and (33), we get the desired result. \blacksquare

5.2 Proof of Theorem 14

The proof of Theorem 14 follows a similar structure to the proof of Theorem 13. However, it requires careful attention to the region where the α -bi-Lipschitz property is not satisfied by the encoder minimizing the GME cost. To prove the theorem, we first define the discrete GME cost function given the discrete measure.

Definition 17. *Given a discrete measure $\hat{\mu}_n = \frac{1}{n} \sum_{i=1}^n \delta_{x_i}$ where $\{x_i\}_{i=1}^n$ are sampled from μ , we define the discrete Gromov-Monge embedding (GME) cost as follows:*

$$\hat{C}_{\text{GME}}(T, \hat{\mu}_n) := \frac{1}{n(n-1)} \sum_{i=1}^n \sum_{j=1}^n \left(\log \left(\frac{1 + \|T(x_i) - T(x_j)\|^2}{1 + \|x_i - x_j\|^2} \right) \right)^2.$$

The following proposition shows the difference between the discrete cost $\hat{C}_{\text{GME}}(T, \hat{\mu}_n)$ and the continuous cost $C_{\text{GME}}(T, \mu)$ is small with high probability given a large number of points.

Proposition 18. *Fix $\beta > 0$ and $\varepsilon > 0$. Let $\hat{\mu}_n = \frac{1}{n} \sum_{i=1}^n \delta_{x_i}$ where $\{x_i\}_{i=1}^n$ are sampled from μ . Suppose $T \in \mathcal{T}_\beta$. Then, the following event*

$$|C_{\text{GME}}(T, \mu) - \hat{C}_{\text{GME}}(T, \hat{\mu}_n)| < B^2 \varepsilon$$

holds with probability at least $1 - 2 \exp\left(-\frac{n\varepsilon^2}{6(1+\varepsilon/3)}\right)$ where B is defined in (7).

Proof We bound $|C_{\text{GME}}(T, \mu) - \hat{C}_{\text{GME}}(T, \hat{\mu}_n)|$ by using Bernstein's inequality for U -statistics (Calder, 2020, Theorem 5.15). We begin by defining the U -statistics

$$U_n = \frac{1}{n(n-1)} \sum_{i \neq j} g(x_i, x_j) \quad (34)$$

where

$$g(x, x') = \left(\log \left(\frac{1 + \|T(x) - T(x')\|^2}{1 + \|x - x'\|^2} \right) \right)^2$$

and we observe that $\hat{C}_{\text{GME}}(T, \hat{\mu}_n) = U_n$. We also note that

$$\mathbb{E}[g(x, x')] = C_{\text{GME}}(T, \mu).$$

Since $T \in \mathcal{T}_\beta$, we have

$$b := \sup_{x, x' \in \mathcal{M}} |g(x, x')| \leq \left(\log(\max(\beta^2, 1 + \text{diam}(\mathcal{M})^2)) \right)^2 =: B^2.$$

Furthermore, the variance is bounded by

$$\sigma^2 \leq \mathbb{E}[g(x, x')^2] = \int_{\mathcal{M}^2} \left(\log \left(\frac{1 + \|T(x) - T(x')\|^2}{1 + \|x - x'\|^2} \right) \right)^4 d\mu(x)d\mu(x) \leq B^4.$$

Using Bernstein's inequality for U -statistics, we have

$$\mathbb{P}\left(|U_n - C_{\text{GME}}(T, \mu)| \geq t\right) \leq 2 \exp\left(-\frac{nt^2}{6(\sigma^2 + bt/3)}\right).$$

Choosing $t = B^2\varepsilon$ and using the bounds for b and σ we have

$$\mathbb{P}\left(|U_n - C_{\text{GME}}(T, \mu)| \geq B^2\varepsilon\right) \leq 2 \exp\left(-\frac{n\varepsilon^2}{6(1 + \varepsilon/3)}\right).$$

This proves the theorem. ■

In Proposition 18, the parameter β represents the least regularity assumption of the encoder T along with the invertibility assumption. To generalize and consider practical scenarios, one can assume β to be close to 0. In this case, we can choose ε to be small and increase the probability of the event holding by increasing the number of points n .

From Proposition 18 and Theorem 3, we can describe the subset of the domain where the α -bi-Lipschitz property is satisfied from the encoder that minimizes the discrete GME cost.

Proposition 19. *Fix $\varepsilon > 0$, $\varepsilon_{\text{GME}} \geq 0$, and $0 < \beta < \alpha \leq 1$. Given a discrete measure $\hat{\mu}_n$, suppose $T \in \mathcal{T}_\beta$ and $\hat{C}_{\text{GME}}(T, \hat{\mu}_n) \leq \varepsilon_{\text{GME}}$. Denote the Lebesgue measure on \mathcal{M} by \mathcal{L} . Then, the following event*

$$\mathcal{L}^2 \left(\left\{ (x, x') \in \mathcal{M}^2 : \alpha^2 \leq \frac{1 + \|T(x) - T(x')\|^2}{1 + \|x - x'\|^2} \leq \frac{1}{\alpha^2} \right\} \right) > 1 - \frac{\varepsilon_{\text{GME}} + B^2\varepsilon}{4\rho_{\min}^2(\log \alpha)^2}$$

holds with probability at least $1 - 2 \exp\left(-\frac{n\varepsilon^2}{6(1+\varepsilon/3)}\right)$ where B is defined in (7).

Proof By Proposition 18, with probability at least $1 - 2 \exp\left(-\frac{n\varepsilon^2}{6(1+\varepsilon/3)}\right)$, we have

$$C_{\text{GME}}(T, \mu) < \varepsilon_{\text{GME}} + B^2\varepsilon.$$

Denote by A the event such that

$$A := \left\{ (x, x') \in \mathcal{M}^2 : \alpha^2 \leq \frac{1 + \|T(x) - T(x')\|^2}{1 + \|x - x'\|^2} \leq \frac{1}{\alpha^2} \right\}.$$

Using Theorem 3 and the assumption in (1), we have

$$\frac{\varepsilon_{\text{GME}} + B^2\varepsilon}{4(\log \alpha)^2} > \mu^2(A^c) \geq \rho_{\min}^2 \mathcal{L}^2(A^c).$$

Thus, rearranging the terms and using $\mathcal{L}^2(A) = 1 - \mathcal{L}^2(A^c)$,

$$\mathcal{L}^2(A) > 1 - \frac{\varepsilon_{\text{GME}} + B^2\varepsilon}{4\rho_{\min}^2(\log \alpha)^2}.$$

This proves the proposition. ■

The following lemma provides an upper bound that allows for comparing the distance between two measures from the data space in D dimensions to the latent space \mathbb{R}^d , which is d dimensions with $d \ll D$, and thus the upper bound is independent of the data space dimension D . This lemma will be crucial in the proof of Theorem 14.

Lemma 20. *Fix $0 < \alpha \leq 1$, $\beta > 0$, $\varepsilon > 0$, $\varepsilon_{\text{GME}} \geq 0$, and $p \geq 1$. Let $\mu, \nu \in \mathbb{P}(\mathcal{M})$ are absolutely continuous measures with respect to the Lebesgue measure \mathcal{L} on \mathcal{M} satisfying the assumption (1) and*

$$d\nu(x) = f(x)d\mathcal{L}(x), \quad f(x) \leq \nu_{\max},$$

for some nonnegative function f and a positive constant ν_{\max} . Let $\hat{\mu}_n = \frac{1}{n} \sum_{i=1}^n \delta_{x_i}$ be an empirical distribution from μ . Let $T \in \mathcal{T}_\beta$ be an embedding map satisfying $\hat{C}_{\text{GME}}(T, \hat{\mu}_n) \leq \varepsilon_{\text{GME}}$. Define a transport plan $\gamma \in \Pi(\hat{\mu}_n, \nu)$ and $\gamma_T \in \Pi(T\#\hat{\mu}_n, T\#\nu)$ such that γ_T is defined as $\gamma_T(x, y) = \gamma(T(x), T(y))$. Then, there exists a positive constant C depending only on p , $\text{diam}(\mathcal{M})$, ρ_{\min} , ρ_{\max} , and ν_{\max} such that the following event

$$\int_{\mathcal{M}^2} \|x-y\|^p d\gamma(x, y) \leq 2^{p-1} \left(\frac{1}{\alpha^p} \int_{(\mathbb{R}^d)^2} \|x-y\|^p d\gamma_T(x, y) + \left(\frac{1}{\alpha^2} - 1 \right)^{p/2} \right) + \frac{C(\varepsilon_{\text{GME}} + B^2\varepsilon)}{(\log \alpha)^2}$$

holds with probability at least $1 - 2 \exp\left(-\frac{n\varepsilon^2}{6(1+\varepsilon/3)}\right)$ where B is defined in Proposition 18.

Proof By Proposition 19, with probability at least $1 - 2 \exp\left(-\frac{n\varepsilon^2}{6(1+\varepsilon/3)}\right)$, there exists a subset $A \subset \mathcal{M}^2$ such that

$$A = \left\{ (x, x') \in \mathcal{M}^2 : \alpha^2 \leq \frac{1 + \|T(x) - T(x')\|^2}{1 + \|x - x'\|^2} \leq \frac{1}{\alpha^2} \right\} \quad (35)$$

and

$$\mathcal{L}^2(A) > 1 - \frac{\varepsilon_{\text{GME}} + B^2\varepsilon}{4\rho_{\min}^2(\log \alpha)^2}. \quad (36)$$

Note that from (35), using the inequality $(a+b)^{1/2} \leq a^{1/2} + b^{1/2}$ for $a, b \geq 0$, one can write

$$\|T^{-1}(x) - T^{-1}(y)\| \leq \frac{1}{\alpha} \|x - y\| + \left(\frac{1}{\alpha^2} - 1 \right)^{1/2}. \quad (37)$$

Then,

$$\int_{\mathcal{M}^2} \|x - y\|^p d\gamma(x, y) = \int_A \|x - y\|^p d\gamma(x, y) + \int_{\mathcal{M}^2 \setminus A} \|x - y\|^p d\gamma(x, y). \quad (38)$$

Using (36), the second term can be bounded above by

$$\begin{aligned} \int_{\mathcal{M}^2 \setminus A} \|x - y\|^p d\gamma(x, y) &\leq \text{diam}(\mathcal{M})^p \int_{\mathcal{M}^2 \setminus A} d\gamma(x, y) \\ &\leq \frac{\text{diam}(\mathcal{M})^p \rho_{\max} \nu_{\max} (\varepsilon_{\text{GME}} + B^2 \varepsilon)}{4\mu_{\min}^2 (\log \alpha)^2}. \end{aligned} \quad (39)$$

Using the definition of a set A , (37), and inequality $(a + b)^p \leq 2^{p-1}(a^p + b^p)$ for $a, b \geq 0$, the first term in (38) can be bounded by

$$\begin{aligned} \int_A \|x - y\|^p d\gamma(x, y) &= \int_{T(A)} \|T^{-1}(x) - T^{-1}(y)\|^p d\gamma_T(x, y) \\ &\leq 2^{p-1} \left(\frac{1}{\alpha^p} \int_{T(A)} \|x - y\|^p d\gamma_T(x, y) + \left(\frac{1}{\alpha^2} - 1 \right)^{p/2} \right) \\ &\leq 2^{p-1} \left(\frac{1}{\alpha^p} \int_{(\mathbb{R}^d)^2} \|x - y\|^p d\gamma_T(x, y) + \left(\frac{1}{\alpha^2} - 1 \right)^{p/2} \right) \end{aligned} \quad (40)$$

where $T(A) := \{(T(x), T(y)) \in (\mathbb{R}^d)^2 : (x, y) \in A\}$ and $\gamma_T \in \Pi(T_{\#}\hat{\mu}_n, T_{\#}\nu)$ is defined by $\gamma_T(x, y) = \gamma(T(x), T(y))$.

Combining (39) and (40), we obtain the desired result. \blacksquare

As a direct consequence of Lemma 20, using the GME encoder, we can bound the Wasserstein distance between the data distribution and any distribution in the data space with dimension D by the Wasserstein distance between the embedded distributions in the latent space with dimension d , with high probability.

Lemma 21. *Under the same assumptions and conditions as in Lemma 20, there exists a positive constant C depending only on p , $\text{diam}(\mathcal{M})$, ρ_{\min} , ρ_{\max} , and ν_{\max} such that the following event*

$$W_p(\hat{\mu}_n, \nu) \leq \frac{2}{\alpha} W_p(T_{\#}\hat{\mu}_n, T_{\#}\nu) + 2 \left(\frac{1}{\alpha^2} - 1 \right)^{1/2} + \frac{C(\varepsilon_{\text{GME}} + B^2 \varepsilon)^{1/p}}{(\log \alpha)^{2/p}}$$

holds with probability at least $1 - 2 \exp\left(-\frac{n\varepsilon^2}{6(1+\varepsilon/3)}\right)$.

Proof From the result in Lemma 20, the term

$$\int_{\mathcal{M}^2} \|x - y\|^p d\gamma(x, y)$$

can be bounded below by $W_p^p(\hat{\mu}_n, \nu)$ by the fact that $\gamma \in \Pi(\hat{\mu}_n, \nu)$ and by the definition of Wasserstein distance. Therefore, we have

$$W_p^p(\hat{\mu}_n, \nu) \leq 2^{p-1} \left(\frac{1}{\alpha^p} \int_{(\mathbb{R}^d)^2} \|x - y\|^p d\gamma_T(x, y) + \left(\frac{1}{\alpha^2} - 1 \right)^{p/2} \right) + \frac{C(\varepsilon_{\text{GME}} + B^2 \varepsilon)}{(\log \alpha)^2}.$$

By applying $\min_{\gamma_T \in \Pi(T_{\#}\hat{\mu}_n, T_{\#}\nu)}$ on both sides, applying power $1/p$, and using the inequality $(a+b)^{1/p} \leq a^p + b^p$ for $a, b \geq 0$, we obtain the desired result. \blacksquare

Now, we are now ready to prove Theorem 14.

Proof of Theorem 14 The proof follows the similar structure as the proof of Theorem 13. Note that, we assume T is a minimizer of $\hat{C}_{\text{GME}}(T, \hat{\mu}_n)$ instead of being assumed as α -bi-Lipshcitz map. Thus, the difference happens when bounding $\|T^{-1}(x) - T^{-1}(y)\|$. From the second line in (29) with $p = 1$, we have

$$\int_{T(\mathcal{M})} \int_{T(\mathcal{M})} \|T^{-1}(x) - T^{-1}(y)\| d\tilde{\gamma}(x, y) = \int_{\mathcal{M}^2} \|x - y\| d\gamma_0(x, y),$$

where $\gamma_0 \in \Pi(\tilde{\mu}, (T^{-1} \circ R)_{\#}\nu)$ and defined as $\gamma_0(x, y) = \tilde{\gamma}(T^{-1}(x), T^{-1}(y))$. By Lemma 20, we have the following event

$$\begin{aligned} & \int_{\mathcal{M}^2} \|x - y\| d\gamma_0 \\ & \leq \frac{1}{\alpha} \int_{(\mathbb{R}^d)^2} \|x - y\| d\tilde{\gamma} + \left(\frac{1}{\alpha^2} - 1\right)^{1/2} + \frac{\text{diam}(\mathcal{M})\rho_{\max} \sup_{x \in \mathcal{M}} (T^{-1} \circ R)_{\#}\nu(x)}{4\mu_{\min}^2 (\log \alpha)^2} (\varepsilon_{\text{GME}} + B^2\varepsilon) \\ & \leq \frac{1}{\alpha} \int_{(\mathbb{R}^d)^2} \|x - y\| d\tilde{\gamma} + \left(\frac{1}{\alpha^2} - 1\right)^{1/2} + \frac{\beta^d \text{diam}(\mathcal{M})\rho_{\max}(R_{\#}\nu)_{\max}}{4\mu_{\min}^2 (\log \alpha)^2} (\varepsilon_{\text{GME}} + B^2\varepsilon) \end{aligned} \quad (41)$$

holds with probability at least $1 - 2 \exp\left(-\frac{n\varepsilon^2}{6(1+\varepsilon/3)}\right)$. In the last inequality, we used

$$(T^{-1} \circ R)_{\#}\nu(x) = \rho_R(T(x)) |\det(\nabla T(x) \nabla T(x)^T)|^{1/2} \leq \beta^d (R_{\#}\nu)_{\max},$$

to have the bound

$$\sup_{y \in \mathcal{M}} (T^{-1} \circ R)_{\#}\nu \leq \beta^d (R_{\#}\nu)_{\max}.$$

Furthermore, following the same argument in (28) and using the assumption that $T \in \mathcal{T}_\beta$, we have

$$\int_{\Omega_d} \|\tilde{S}(y) - S(y)\|^2 dR_{\#}\nu \leq \frac{(R_{\#}\nu)_{\max} \beta^d}{\rho_{\min}} (\varepsilon_{\text{rec}} + \text{diam}(\mathcal{M}^2)\varepsilon) \quad (42)$$

holds with probability at least $1 - 2 \exp\left(-\frac{n\varepsilon^2}{6(1+\varepsilon/3)}\right)$.

Going back to (29), and combining with (41) and (42), we obtain the following event

$$\begin{aligned} & W_1(\hat{\mu}_n, (S \circ R)_{\#}\nu) \\ & \leq \frac{1}{\alpha} \int_{(\mathbb{R}^d)^2} \|x - y\| d\tilde{\gamma} + \left(\frac{1}{\alpha^2} - 1\right)^{1/2} + C_1 \beta^d \left(\frac{\varepsilon_{\text{GME}} + B^2\varepsilon}{(\log \alpha)^2} + \varepsilon_{\text{rec}} + \varepsilon \right) \\ & \quad + \text{diam}(\mathcal{M}) R_{\#}\nu(\Omega_d \setminus T(\mathcal{M})) \end{aligned}$$

holds with probability at least $1 - 4 \exp\left(-\frac{n\varepsilon^2}{6(1+\varepsilon/3)}\right)$ where C_1 is a positive constant depending on $\text{diam}(\mathcal{M})$, ρ_{\min} , ρ_{\max} , and $(R_{\#\nu})_{\max}$. By applying $\min_{\tilde{\gamma} \in \Pi(T_{\#}\hat{\mu}_n, R_{\#\nu})}$ on both sides and using (21) and the inequality $W_1(\mu, \nu) \leq W_p(\mu, \nu)$ for any probability measures μ, ν and $p \geq 1$, we obtain

$$\begin{aligned} & W_1(\hat{\mu}_n, (S \circ R)_{\#\nu}) \\ & \leq \frac{\varepsilon_{\text{dif}}}{\alpha} + \left(\frac{1}{\alpha^2} - 1\right)^{1/2} + C_1 \beta^d \left(\frac{\varepsilon_{\text{GME}} + B^2 \varepsilon}{(\log \alpha)^2} + \varepsilon_{\text{rec}} + \varepsilon \right) + \text{diam}(\mathcal{M}) R_{\#\nu}(\Omega_d \setminus T(\mathcal{M})). \end{aligned} \quad (43)$$

Next we will relate (43) with $W_1(\mu, (S \circ R)_{\#\nu})$. Note that, using the triangle inequality property of the Wasserstein-1 distance, we have

$$W_1(\mu, (S \circ R)_{\#\nu}) \leq W_1(\hat{\mu}_n, (S \circ R)_{\#\nu}) + W_1(\mu, \hat{\mu}_n). \quad (44)$$

Using Lemma 21, we can bound the second term by

$$W_1(\mu, \hat{\mu}_n) \leq \frac{1}{\alpha} W_1(T_{\#}\mu, T_{\#}\hat{\mu}_n) + \left(\frac{1}{\alpha^2} - 1\right)^{1/2} + \frac{C_2(\varepsilon_{\text{GME}} + B^2 \varepsilon)}{(\log \alpha)^2}$$

where C_2 is a positive constant depending only on $\text{diam}(\mathcal{M})$, ρ_{\min} , and ρ_{\max} . By applying the expectation over samples and using the result from Horowitz and Karandikar (1994), we have

$$\begin{aligned} \mathbb{E}W_1(\mu, \hat{\mu}_n) & \leq \frac{1}{\alpha} \mathbb{E}W_1(T_{\#}\mu, T_{\#}\hat{\mu}_n) + \left(\frac{1}{\alpha^2} - 1\right)^{1/2} + \frac{C_2(\varepsilon_{\text{GME}} + B^2 \varepsilon)}{(\log \alpha)^2} \\ & \leq \frac{C_3 n^{-2/(d+4)}}{\alpha} + \left(\frac{1}{\alpha^2} - 1\right)^{1/2} + \frac{C_2(\varepsilon_{\text{GME}} + B^2 \varepsilon)}{(\log \alpha)^2} \end{aligned} \quad (45)$$

where C_3 depends only on $T_{\#}\mu$ and d .

Combining (43), (44), and (45), we have

$$\begin{aligned} & W_1(\mu, (S \circ R)_{\#\nu}) \\ & \leq C_4 \beta^d \left(\frac{\varepsilon_{\text{GME}} + B^2 \varepsilon}{(\log \alpha)^2} + \varepsilon_{\text{rec}} + \varepsilon \right) + \frac{1}{\alpha} \left(\varepsilon_{\text{dif}} + C_3 n^{-2/(d+4)} + 2(1 - \alpha^2)^{1/2} \right) \\ & \quad + \text{diam}(\mathcal{M}) R_{\#\nu}(\Omega_d \setminus T(\mathcal{M})) \end{aligned}$$

holds with probability at least $1 - 4 \exp\left(-\frac{n\varepsilon^2}{6(1+\varepsilon/3)}\right)$ where C_4 is a positive constant depending on $\text{diam}(\mathcal{M})$, ρ_{\min} , ρ_{\max} , and $(R_{\#\nu})_{\max}$. This completes the proof. \blacksquare

6 Algorithm

In this section, we outline the algorithms for computing the geometry-preserving encoder $T : \mathcal{M} \rightarrow \mathbb{R}^d$ (Algorithm 1) and the decoder $S : \mathbb{R}^d \rightarrow \mathcal{M}$ (Algorithm 2).

6.1 Algorithm for the GPE encoder

Let’s delve into the details of the first part of the algorithm. Given a data distribution $\mu \in \mathbb{P}(\mathcal{M})$, the initial step aims to compute the geometry-preserving encoder $T : \mathcal{M} \rightarrow \mathbb{R}^d$ by solving the optimization problem in (3). Let T_{w_T} be a neural network function that approximates the map T , where w_T is a vector of neural network parameters. The algorithm is presented in Algorithm 1.

Algorithm 1 Computing the GPE encoder

Input: Data distribution $\mu \in \mathbb{P}(\mathcal{M})$, latent dimension d , tolerance TOL, learning rate σ .
Output: GPE encoder $T_{w_T} : \mathcal{M} \rightarrow \mathbb{R}^d$.
while $C_{\text{GME}}(T_{w_T}, \mu) > \text{TOL}$ **do**
 $w_T \leftarrow w_T - \sigma \nabla_{w_T} C_{\text{GME}}(T_{w_T}, \mu)$.
end while

6.2 Algorithm for the GPE decoder

Now, we present the algorithm for computing the decoder $S : \mathbb{R}^d \rightarrow \mathcal{M}$ which is an inverse map $S = T^{-1}$. Let S_{w_S} be a neural network function approximating the map S , where w_S is a vector of neural network parameters. By employing a simple L^2 loss function,

$$L_{\text{rec}}(S) = \mathbb{E}_{x \sim \mu} [\|x - S_{w_S}(T_{w_T}(x))\|^2], \quad (46)$$

we can compute the decoder S . The algorithm is presented in Algorithm 2.

Algorithm 2 Computing the GPE decoder

Input: Data distribution $\mu \in \mathbb{P}(\mathcal{M})$, an encoder $T_{w_T} : \mathcal{M} \rightarrow \mathbb{R}^d$, tolerance TOL, learning rate σ .
Input: GPE decoder $S_{w_S} : \mathbb{R}^d \rightarrow \mathcal{M}$ such that $S_{w_S} = T_{w_T}^{-1}$.
while $L_{\text{rec}}(S_{w_S}) > \text{TOL}$ **do**
 $w_S \leftarrow w_S - \sigma \nabla_{w_S} L_{\text{rec}}(S_{w_S})$.
end while

Here, $c_{\min} = c_{\max} = 2$ due to the choice of the cost function in (46). Thus, the step size σ in Algorithm 2 depends only on α and ρ_{\max} by Theorem 11. Although ρ_{\max} is unknown in practice, we can still infer that if $C_{\text{GME}}(T, \mu)$ is small from Algorithm 1, one can choose a higher step size.

7 Numerical results

In this section, we present numerical experiments demonstrating the effectiveness of our proposed method across various datasets, highlighting its efficiency in both reconstruction and generation tasks compared to other methods.

7.1 Visualization of encoder differences in GPE and VAE

In this experiment, our goal is to visualize the differences between the encoders from GPE and VAE. The primary objective of the GPE encoder is to embed the data distribution while preserving its geometric structure, whereas the VAE encoder aims to map the data distribution to a Gaussian distribution in the latent space.

To demonstrate this, we use artificial datasets in 500 dimensions consisting of a mixture of Gaussians. The covariance matrix of each Gaussian is diagonal, with the first two diagonal entries being 0.15^2 and the rest 10^{-4} . This setup represents a dataset lying on a manifold in the first two dimensions of the ambient space, with small noise in the other dimensions. We train both GPE and VAE encoders using a 4-layer fully-connected neural network.

The results are displayed in Figure 3. The first column shows the input data distribution in \mathbb{R}^{500} by plotting the first two coordinates in a cross-section, while the second and third columns show the embedded distributions on \mathbb{R}^2 from the trained GPE and VAE encoders, respectively. As expected, the GPE encoder preserves the geometric structure of the original data distribution, whereas the VAE encoder maps the distribution onto a Gaussian distribution, which illustrates the posterior collapse phenomenon (Wang et al., 2021b). Although the VAE results still show some geometric structure, the GPE encoder better preserves the geometric structure of the data distribution.

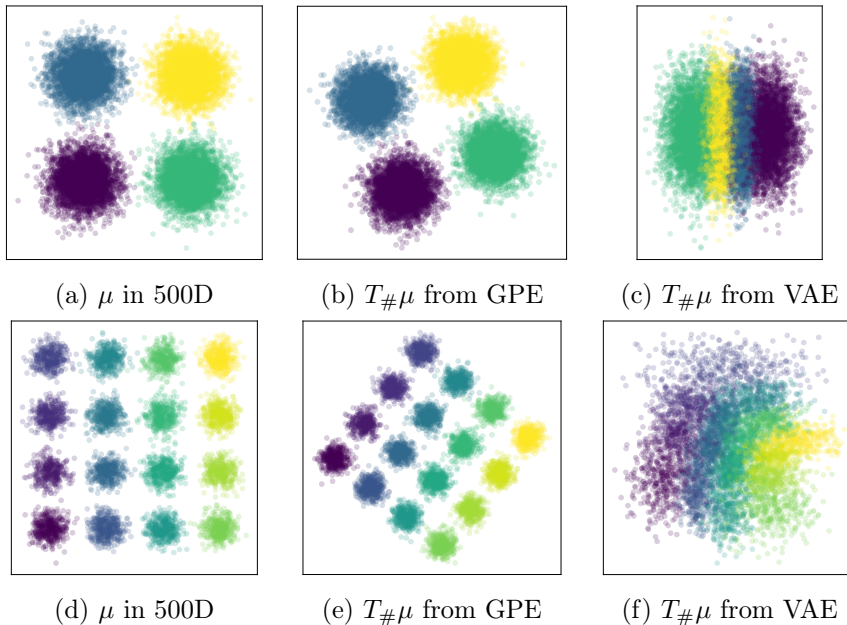


Figure 3: Comparison of embedded data distributions from GPE and VAE. The first column shows the input data distribution μ in 500D, while the second and third columns show the embedded distributions $T_{\#}\mu$ from GPE and VAE, respectively, in 2D.

7.2 Optimization efficiency with GPE encoders

Throughout the experiments, we implement the algorithm on real-world datasets. Specifically, we use the MNIST (Deng, 2012), CIFAR10 (Krizhevsky et al., 2009), CelebA (Liu et al., 2015), and CelebA-HQ (256×256) (Karras et al., 2017) datasets to demonstrate the efficiency of the GPE framework compared to the VAE framework in terms of reconstruction and generation tasks.

In this experiment, we demonstrate the efficiency of the optimization process for computing the decoder while considering the geometry-preserving property of the encoder, as established in Theorem 11. Specifically, we illustrate that the computation of the decoder becomes more efficient and faster as the encoder’s bi-Lipschitz constant α approaches 1. For this experiment, we utilize the CIFAR10 dataset.

We employ three distinct encoders, each computed using Algorithm 1 and the GME cost, with training stopped at three difference TOL values as indicated in Figure 4. We use the same neural network architectures for encoders and the same learning rate $lr = 10^{-4}$ and batch size 100.

Using each pretrained encoder with a different value of TOL, we use Algorithm 2 to minimize the cost in (46). Figure 4 displays the loss plots for the first 5,000 iterations. We use the same neural network architectures for decoders and the same learning rate $lr = 10^{-4}$ and batch size 100. The figure clearly illustrates the relationship between optimization efficiency and the level of geometry preservation exhibited by the encoder.

7.3 Comparison of reconstruction task efficiency between GPE and VAE Frameworks

In this experiment, we compare the efficiency of reconstruction tasks by training the encoders and decoders from both the VAE and GPE frameworks, using the same neural network architectures for both. To evaluate performance, we first train the encoders from both frameworks. Using the pre-trained encoders, we then separately train the decoders using only the reconstruction cost and assess the efficiency and performance of the training optimization results.

Note that, unlike GPE, where the optimization process involves the encoder independently of the decoder, VAE requires training both the encoder and decoder simultaneously using the ELBO loss. Therefore, to obtain the pre-trained encoders for VAE, we first train both the encoder and decoder. Afterward, we freeze the VAE encoder, ignore the trained decoder, and train a new decoder from scratch. This allows us to compare the optimization process of minimizing solely the reconstruction loss for decoders from both frameworks.

The results, shown in Table 1, indicate the iterations required for each method to reach the specified loss value. For GPE, the third column includes the value of TOL used in Algorithm 1. All parameters, including learning rates and neural network architectures for both the encoder and decoder, are identical across datasets. The results for GPE were obtained using two A40 GPUs, while two A100 GPUs were for VAE.

The numerical results indicate a reduction in the number of training iterations required by GPE compared to VAE across all datasets. Specifically, some datasets exhibit a substantial improvement, with iteration reductions ranging from 3 times (CelebA) to 900 times (MNIST) with the given loss thresholds. Notably, the discrepancy in the number of itera-

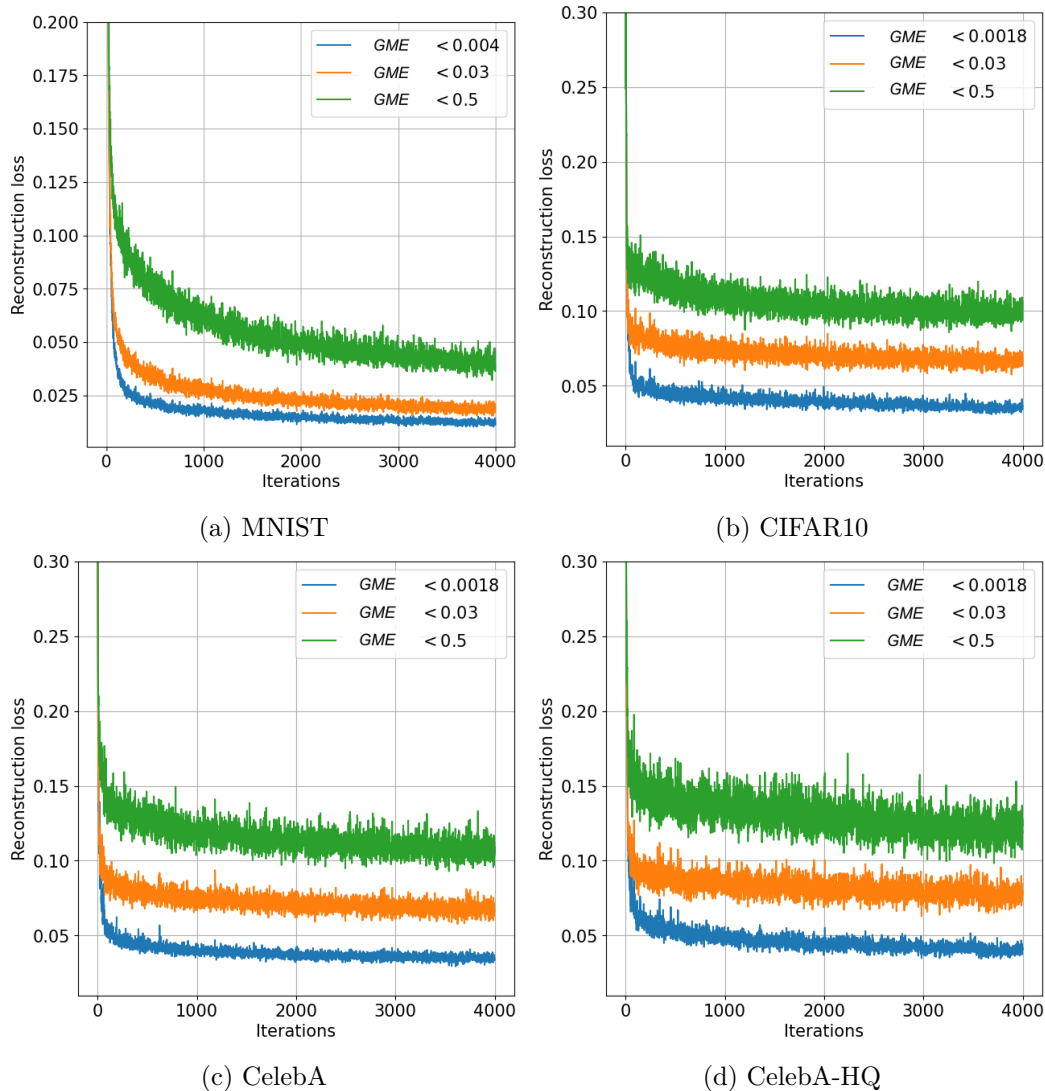


Figure 4: The plots illustrate the results of minimizing the reconstruction loss in (46) on four datasets, MNIST, CIFAR10, CelebA, and CelebA-HQ using three different encoders, each characterized by a different tolerance values.

tions becomes more pronounced as the loss threshold is decreased. For instance, in the case of CelebA, GPE converges to a loss value of 0.005 within 225,000 iterations, whereas VAE fails to converge to this loss even after 700,000 iterations.

However, the performance on the CelebA-HQ dataset is similar for both VAE and GPE. This can be explained by the fact that, although CelebA-HQ resides in a higher-dimensional space ($\mathbb{R}^{256 \times 256 \times 3}$), it only consists of 30,000 images, which is much smaller in size compared to CelebA, which contains over 200,000 images. We believe this smaller dataset size allows for easier convergence of the decoder to a lower reconstruction loss.

The visualization of the convergence of the optimization process for minimizing the reconstruction cost is shown in Figure 5, and the results of the reconstructed images from GPE and VAE are displayed in Figure 6. Figure 7 highlights the notable difference in reconstruction performance between VAE and GPE, clearly showing better performance from GPE.

Pretrained Encoder	Encoder iterations	TOL	Decoder iterations	Decoder iterations
MNIST (Latent dimensions: 30)			Loss: 0.1	Loss: 0.022
VAE	2,700,000	N/A	80	280,899
GPE	3,800	0.03	47	1,044
GPE	16,000	0.004	47	308
CIFAR10 (Latent dimensions: 100)			Loss: 0.1	Loss: 0.015
VAE	1,250,000	N/A	37	159,036
GPE	2,700	0.03	19	64,281
GPE	23,700	0.0009	19	11,071
CelebA (Latent dimensions: 100)			Loss: 0.1	Loss: 0.015
VAE	1,215,000	N/A	28	120,497
GPE	66,000	0.0007	20	40,023
CelebA-HQ (Latent dimensions: 100)			Loss: 0.1	Loss: 0.0045
VAE	180,000	N/A	23	105,178
GPE	141,100	0.0007	21	104,129

Table 1: Comparison of training decoders from pretrained encoders on various datasets

7.4 Comparison of latent generative task efficiency between GPE and VAE Frameworks

In this experiment, we aim to compare the performance of latent generative tasks between the GPE and VAE frameworks. Given pre-trained encoders and decoders from both models, we train the diffusion model to compute a flow map $R : \mathbb{R}^d \rightarrow \mathbb{R}^d$ such that $R_{\#}\nu \approx T_{\#}\mu$, where ν is the latent distribution and μ is the embedded data distribution generated by the encoder T . Notably, the flow map R is computed using the same neural network architectures for both frameworks. We employ the conditional flow matching algorithm (Lipman et al., 2022) to compute R , and the Fréchet Inception Distance (FID) score (Heusel et al., 2017) is used to assess the quality of the generated samples, calculated from five sets of 5000 fake samples versus 5000 real samples.

The results are shown in Table 2, where it can be seen that the FID scores are similar for both frameworks. While all the other data show similar performance for VAE and GPE, a notable difference can be found in CelebA. Specifically, the FID score for VAE after 1.7 million iterations of training is about 4.24, whereas the FID score for GPE after 400,000 iterations is about 1.24, which is significantly better than VAE. This difference is due to the fact that training VAE on the CelebA dataset was challenging, as can also be seen in Table 1, where a large number of iterations are required to reach the desired

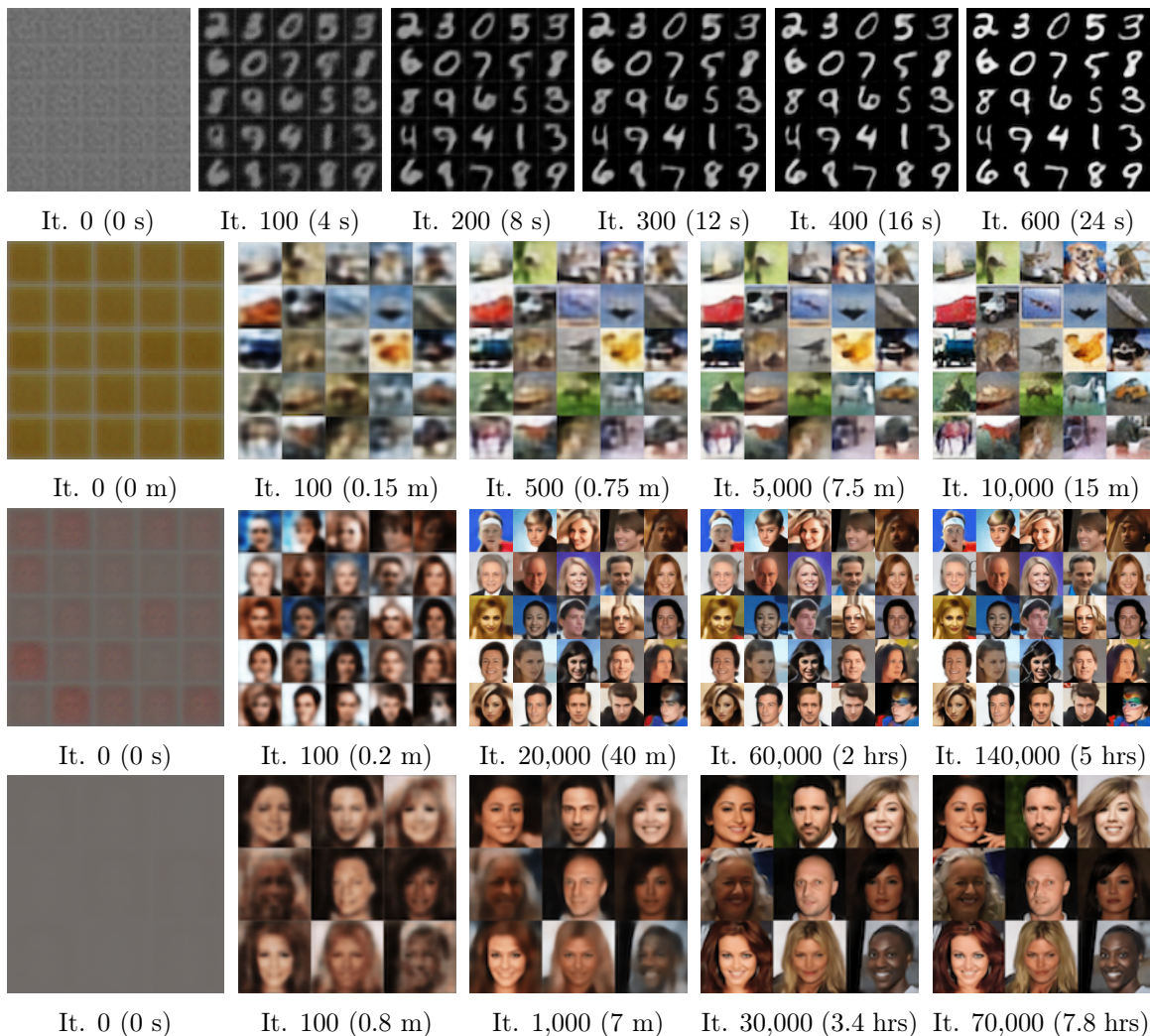


Figure 5: Convergence of training a decoder G using a geometry-preserving encoder with various datasets: first row (MNIST), second row (CIFAR10), third row (CelebA), and fourth row (CelebA-HQ). Each figure caption shows the iteration number and the time taken in seconds (s) and minutes (m). Different neural network architectures for the decoder were used for each dataset. All experiments were done with the same GPU settings: 2 A40 GPUs.

reconstruction loss. Furthermore, as mentioned previously, even if VAE is trained for longer, its reconstruction loss does not decrease beyond a certain point, whereas GPE continues to improve its reconstruction loss, leading to better performance. This explains the difference in FID scores between the two models, with GPE showing better generation performance due to its superior reconstruction performance.

Additionally, note that, from Table 2, for VAE, the FID score starts low and increases, then decreases over the course of training. This behavior is due to the fact that when VAE is trained, the embedded distribution $T_{\text{VAE}\#\mu}$ is expected to resemble a Gaussian in the latent space (see Figure 3). As a result, the goal is to compute a flow map from a Gaussian

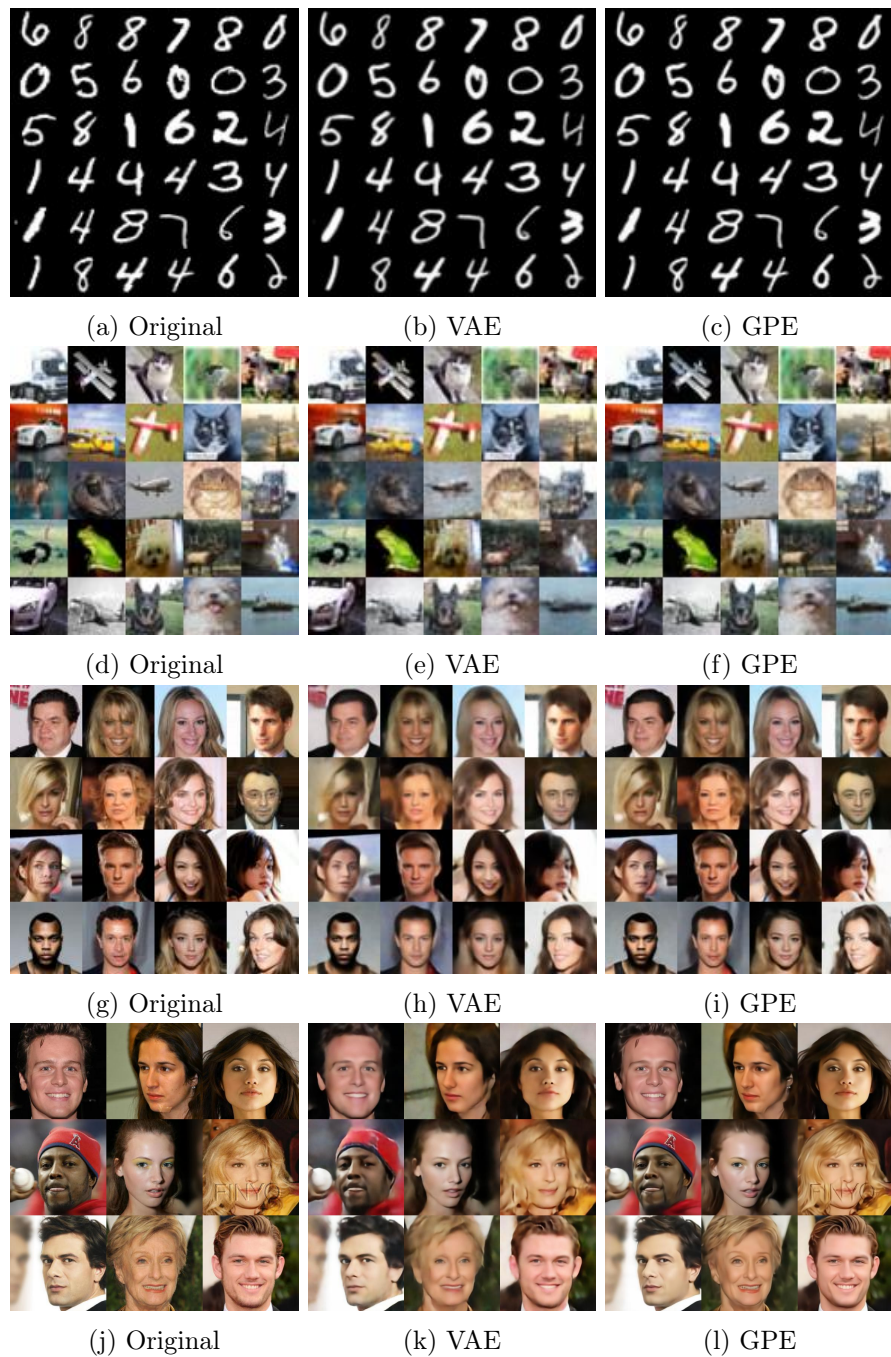


Figure 6: The figure shows the original images (left column), the corresponding reconstructed images from the VAE (center column), and those from the GPE (right column). The datasets used are CIFAR10 (a) - (c), CelebA (d) - (f), and CelebA-HQ (256×256) (g) - (i).

distribution to the embedded distribution, similar to the Gaussian distribution. The ideal flow map is similar to the identity map, where $R(x) \approx x$. However, during the training of the



Figure 7: Examples of reconstructed images from CelebA-HQ, as shown in Figure 6, highlighting the clear distinction between VAE and GPE reconstructed images, presented alongside the original image.

flow map in diffusion models, including the conditional flow matching algorithm, the flow map deviates from the identity map and converges to the map that solves the conditional flow matching algorithm. This explains the initial increase in the FID score followed by its subsequent decrease.

On the other hand, for GPE, since the embedded distribution is not related to the Gaussian distribution, the FID score at iteration 0 is high. However, as training progresses, the FID score decreases because the algorithm learns the flow map that transforms the Gaussian distribution into the embedded distribution, resulting in a decreasing trend in FID scores over training iterations.

8 Conclusion

In this paper, we presented a novel encoder/decoder framework that can be implemented on LGMs. The key finding is that training efficiency in terms of accuracy and speed can be drastically improved by considering the geometry-preserving property of the encoder. These findings are supported by both theoretical analysis and numerical experiments. Future research directions may include implementing the GPE framework on Large Language Models (LLMs), where the transformer model uses an encoder/decoder framework, making it a natural consideration. Furthermore, we may also explore multi-modal generative modeling problems using both text and images.

Acknowledgments and Disclosure of Funding

WL acknowledges funding from the National Institute of Standards and Technology (NIST) under award number 70NANB22H021. RCWO was supported by NSF GRFP-2237827 and NSF-DMS:1944925. DZ acknowledge funding from the Kunshan Municipal Government research funding. JC was supported by NSF-DMS:1944925, NSF-CCF:2212318, the Alfred P. Sloan Foundation, and the Albert and Dorothy Marden Professorship, and GL

		VAE		GPE	
Dataset	Latent Dimension	FID	It (K)	FID	It (K)
MNIST	30	0.65 ± 0.14	0	106.40 ± 0.77	0
		0.54 ± 0.03	10	2.22 ± 0.17	10
		0.56 ± 0.04	30	1.13 ± 0.11	30
		0.59 ± 0.04	60	0.57 ± 0.07	150
CIFAR10	100	1.16 ± 0.13	0	97.03 ± 3.06	0
		1.42 ± 0.11	10	8.89 ± 0.88	10
		1.42 ± 0.08	50	3.79 ± 0.37	50
		1.21 ± 0.05	150	1.27 ± 0.26	200
CelebA	100	3.37 ± 0.38	0	121.30 ± 1.21	0
		14.7 ± 0.64	100	5.82 ± 0.65	100
		6.10 ± 0.52	1,000	2.79 ± 0.59	200
		4.24 ± 0.37	1,700	1.24 ± 0.08	400
CelebA-HQ	100	3.88 ± 0.12	0	82.65 ± 2.01	0
		4.15 ± 0.43	100	7.46 ± 0.59	100
		3.03 ± 0.22	200	3.91 ± 0.46	200
		2.30 ± 0.29	500	2.32 ± 0.24	500

Table 2: Comparison of FID scores and total training iterations between two different encoder/decoder frameworks, VAE and GPE, across various datasets. Conditional flow matching algorithm was used as the diffusion model in the latent space.

acknowledges funding from NSF award DMS 2124913. We are grateful to the Minnesota Super-computing Institute for allowing use of their computational resources.

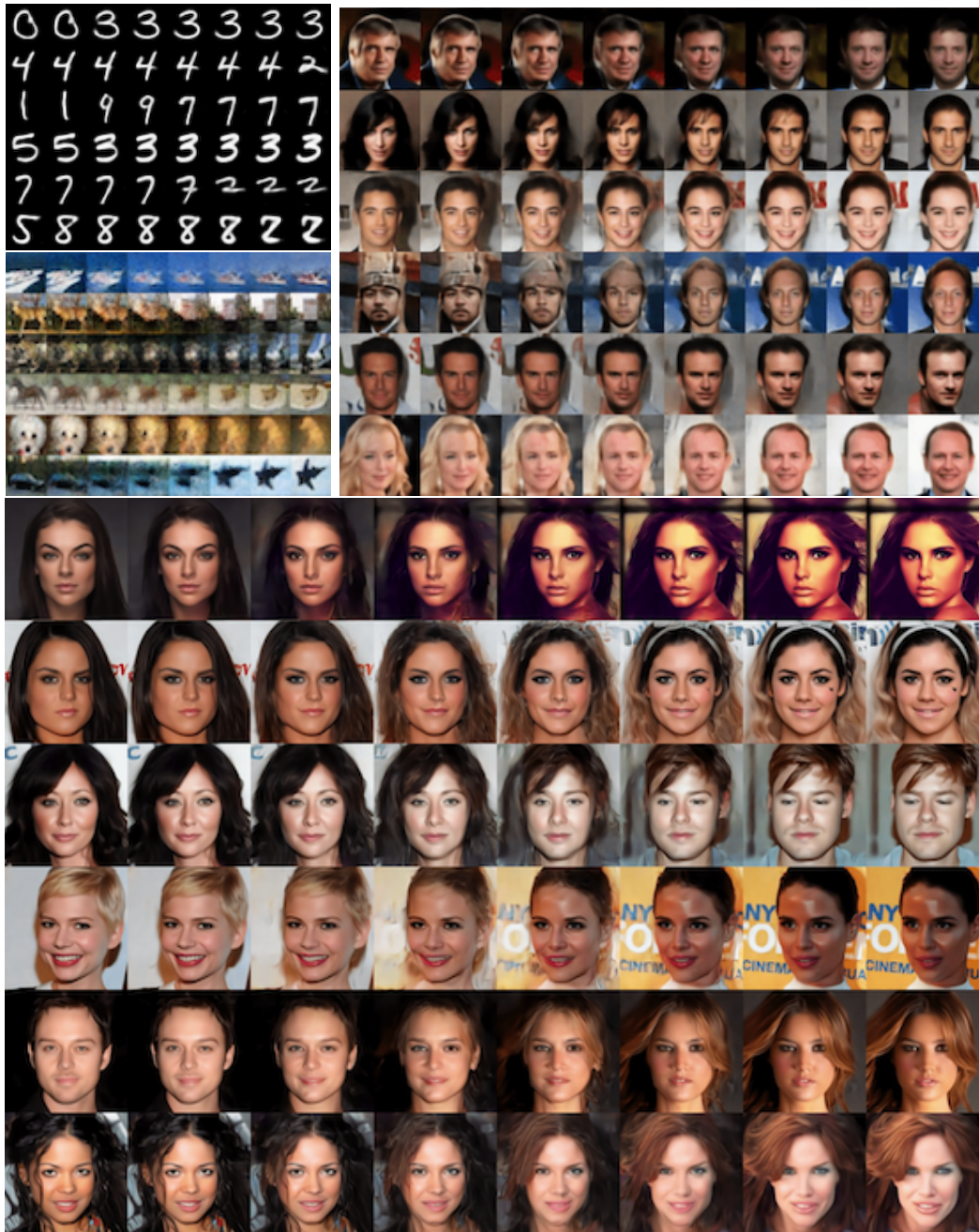


Figure 8: The figure shows the generation results from the GPE-based LGM. Using the diffusion model (specifically the conditional flow matching model) trained in the latent space, the interpolation between two images is generated for various datasets, including MNIST (top left, 1st row), CIFAR10 (top left, 2nd row), CelebA (top right), and CelebA-HQ (256×256 , bottom). The training times for the encoder/decoder and diffusion model for all datasets are displayed in Table 1 and Table 2.

Appendix

Appendix A. Proof of Proposition 8

To derive the second variation of GME cost, we will assume general form on cost functions c_X and c_Y . Throughout the proofs, we assume the cost functions c_X and c_Y take the form

$$c_X(x, x') = \eta_X(x - x'), \quad c_Y(y, y') = \eta_Y(y - y')$$

where $\eta_X : X \rightarrow \mathbb{R}$ and $\eta_Y : Y \rightarrow \mathbb{R}$ are differentiable functions. In the following, for simplicity, we denote by

$$\begin{aligned} \eta_X &= \eta_X(x - x') \\ \eta_Y &= \eta_Y(T(x) - T(x')) \\ \nabla \eta_Y &= \nabla \eta_Y(T(x) - T(x')) \\ \nabla^2 \eta_Y &= \nabla^2 \eta_Y(T(x) - T(x')) \\ h_{x,x'} &= h(x) - h(x'). \end{aligned}$$

Thus, the GME cost can be written as

$$C_{\text{GME}}(T, \mu) = \int_{\mathcal{M}^2} (\eta_X - \eta_Y)^2 d\mu d\mu.$$

Proposition 22. *The first and second variations of the GME cost functional at $T : \mathcal{M} \rightarrow \mathbb{R}^d$ in the direction of $h : \mathcal{M} \rightarrow \mathbb{R}^d$ take the form*

$$\delta C_{\text{GME}}(T, \mu)(h) = 2 \int_{\mathcal{M}^2} (\eta_Y - \eta_X) \langle \nabla \eta_Y, h_{x,x'} \rangle d\mu(x) d\mu(x')$$

and

$$\delta^2 C_{\text{GME}}(T, \mu)(h, h) = 2 \int_{\mathcal{M}^2} \langle \nabla \eta_Y, h_{x,x'} \rangle^2 + (\eta_Y - \eta_X) \langle \nabla^2 \eta_Y h_{x,x'}, h_{x,x'} \rangle d\mu(x) d\mu(x').$$

respectively.

Proof Let $h : \mathcal{M} \rightarrow \mathbb{R}^d$ be a function, and let $t \in \mathbb{R}$. Since η_Y is assumed to be differentiable, it follows that

$$\eta_Y((T + th)_{x,x'}) = \eta_Y(T_{x,x'} + th_{x,x'}) = \eta_Y + t \langle \nabla \eta_Y, h_{x,x'} \rangle + O(t^2). \quad (47)$$

Using (47), we have

$$\begin{aligned} & C_{\text{GME}}(T + th; \mu) \\ &= \int_{\mathcal{M}^2} (\eta_X - \eta_Y((T + th)_{x,x'}))^2 d\mu(x) d\mu(x') \\ &= \int_{\mathcal{M}^2} (\eta_X - \eta_Y - t \langle \nabla \eta_Y, h_{x,x'} \rangle + O(t^2))^2 d\mu(x) d\mu(x') \\ &= \int_{\mathcal{M}^2} (\eta_X - \eta_Y)^2 - t \left(2(\eta_X - \eta_Y) \langle \nabla \eta_Y, h_{x,x'} \rangle \right) d\mu(x) d\mu(x') + O(t^2). \end{aligned}$$

From the definition of the first variation in (8), we get the formulation for $\delta C_{\text{GME}}(T, \mu)(h)$.

Next, we compute the second variation. For any $t \in \mathbb{R}$, using (47) and the first variation $\delta \text{GM}(T, \mu)$,

$$\begin{aligned} & \delta C_{\text{GME}}(T + th)(h) \\ &= 2 \int_{\mathcal{M}^2} \left(\eta_Y + t \langle \nabla \eta_Y, h_{x,x'} \rangle + O(t^2) - \eta_X \right) \left\langle \nabla \eta_Y + t \nabla^2 \eta_Y h_{x,x'} + O(t^2), h_{x,x'} \right\rangle d\mu(x) d\mu(x') \\ &= 2 \int_{\mathcal{M}^2} (\eta_Y - \eta_X) \langle \nabla \eta_Y, h_{x,x'} \rangle + t \langle \nabla \eta_Y, h_{x,x'} \rangle^2 \\ & \quad + t (\eta_Y - \eta_X) \langle \nabla^2 \eta_Y h_{x,x'}, h_{x,x'} \rangle d\mu(x) d\mu(x') + O(t^2). \end{aligned}$$

From the definition of the second variation in (9), we get the formulation for $\delta^2 C_{\text{GME}}(T, \mu)(h, h)$. This concludes the proof. \blacksquare

Using Proposition 22, by plugging in $\eta_X(x - x') = \log(1 + \|x - x'\|^2)$ and $\eta_Y(y - y') = \log(1 + \|y - y'\|^2)$, we get the second variation in Proposition 8. \square

Appendix B. Proof of Corollary 10

The proof follows a standard optimization proof for gradient descent convergence. For simplicity, let us omit μ and write $F(T) = C_{\text{GME}}(T, \mu)$. From the second-order approximation of $C_{\text{GME}}(T, \mu)$ and using the upper bound of the Hessian from Theorem 9 and (17), we have:

$$\begin{aligned} F(T^{(k+1)}) &\leq F(T^{(k)}) + \delta F(T^{(k)})(T^{(k+1)} - T^{(k)}) + \frac{L}{2} \|T^{(k+1)} - T^{(k)}\|_{L^2(\mathcal{M})}^2 \\ &\leq F(T^{(k)}) - \sigma \|\nabla_{L^2} F(T^{(k)})\|_{L^2(\mathcal{M})}^2 + \frac{\sigma^2 L}{2} \|\nabla_{L^2} F(T^{(k)})\|_{L^2(\mathcal{M})}^2 \end{aligned} \quad (48)$$

where L is an upper bound of the hessian defined as $L = 8(2 \log(1 + \beta^2 \text{diam}(\mathcal{M})^2) + 1)$. Note that the L^2 gradient of a function in $L^2(\mathcal{M})$ and the first variation are related by

$$\langle \nabla_{L^2} F(T), h \rangle_{L^2(\mathcal{M})} = \delta F(T)(h), \quad \forall h : \mathcal{M} \rightarrow \mathbb{R}^d.$$

For simplicity, we will omit L^2 in the gradient notation and write $\nabla = \nabla_{L^2}$.

By choosing $\sigma = \frac{1}{L}$ in (48) and rearranging terms, we have

$$F(T^{(k)}) - F(T^{(k+1)}) \geq \frac{1}{2L} \|\nabla F(T^{(k)})\|_{L^2(\mathcal{M})}^2.$$

Summing over $k = 0, \dots, K - 1$, we have

$$F(T^{(0)}) - F(T^{(K)}) \geq \frac{1}{2L} \sum_{i=0}^{K-1} \|\nabla F(T^{(i)})\|_{L^2(\mathcal{M})}^2 \geq \frac{K}{2L} \min_{k < K} \|\nabla F(T^{(k)})\|_{L^2(\mathcal{M})}^2.$$

This completes the proof. \square

Appendix C. Proof of Theorem 12

Consider a domain $\Omega \subset \mathbb{R}^D$ and a function $f : \Omega \rightarrow \mathbb{R}$ that is ℓ -strongly convex with $\ell > 0$:

$$f(y) \geq f(x) + \langle \nabla f(x), y - x \rangle + \frac{\ell}{2} \|y - x\|^2 \quad \forall x, y \in \Omega,$$

and L -smooth:

$$\|\nabla f(x) - \nabla f(y)\| \leq L\|x - y\|, \quad \forall x, y \in \Omega.$$

The convergence rate of the gradient descent iterations follows:

$$\|x^{(k)} - x^{(*)}\| \leq (1 - \sigma\ell)^k \|x^{(0)} - x^{(*)}\|,$$

where $x^{(*)}$ is the minimizer of f and $\sigma > 0$ is the step size of the iteration satisfying $\sigma \leq 1/L$. By applying $\ell = \alpha^d c_{\min} \rho_{\min}$ and $L = \frac{c_{\max} \rho_{\max}}{\alpha^d}$, we obtain the desired result. \square

References

- A. Alemi, B. Poole, I. Fischer, J. Dillon, R. A. Saurous, and K. Murphy. Fixing a broken elbo. In *International conference on machine learning*, pages 159–168. PMLR, 2018.
- D. Alvarez-Melis and T. Jaakkola. Gromov-Wasserstein alignment of word embedding spaces. pages 1881–1890, Oct.-Nov. 2018. doi: 10.18653/v1/D18-1214. URL <https://aclanthology.org/D18-1214>.
- A. Asperti and M. Trentin. Balancing reconstruction error and kullback-leibler divergence in variational autoencoders. *Ieee Access*, 8:199440–199448, 2020.
- Y. Bengio, A. Courville, and P. Vincent. Representation learning: A review and new perspectives. *IEEE transactions on pattern analysis and machine intelligence*, 35(8):1798–1828, 2013.
- C. Bunne, D. Alvarez-Melis, A. Krause, and S. Jegelka. Learning generative models across incomparable spaces. In *International conference on machine learning*, pages 851–861. PMLR, 2019.
- J. Calder. The calculus of variations. *University of Minnesota*, 40, 2020.
- J. D. Carroll and P. Arabie. Multidimensional scaling. *Measurement, judgment and decision making*, pages 179–250, 1998.
- X. Chen, C. Wang, X. Lan, N. Zheng, and W. Zeng. Neighborhood geometric structure-preserving variational autoencoder for smooth and bounded data sources. *IEEE Transactions on Neural Networks and Learning Systems*, 33(8):3598–3611, 2021.
- M. Connor, G. Canal, and C. Rozell. Variational autoencoder with learned latent structure. In *International conference on artificial intelligence and statistics*, pages 2359–2367. PMLR, 2021.
- Q. Dao, H. Phung, B. Nguyen, and A. Tran. Flow matching in latent space. *arXiv preprint arXiv:2307.08698*, 2023.

- L. Deng. The mnist database of handwritten digit images for machine learning research. *IEEE Signal Processing Magazine*, 29(6):141–142, 2012.
- L. Falorsi, P. de Haan, T. R. Davidson, and P. Forré. Reparameterizing distributions on lie groups. In *The 22nd International Conference on Artificial Intelligence and Statistics*, pages 3244–3253. PMLR, 2019.
- R. Gao, X. Hou, J. Qin, J. Chen, L. Liu, F. Zhu, Z. Zhang, and L. Shao. Zero-VAE-GAN: Generating unseen features for generalized and transductive zero-shot learning. *IEEE Transactions on Image Processing*, 29:3665–3680, 2020.
- A. Gropp, M. Atzmon, and Y. Lipman. Isometric autoencoders. *arXiv preprint arXiv:2006.09289*, 2020.
- S. Gu, D. Chen, J. Bao, F. Wen, B. Zhang, D. Chen, L. Yuan, and B. Guo. Vector quantized diffusion model for text-to-image synthesis. In *Proceedings of the IEEE/CVF conference on computer vision and pattern recognition*, pages 10696–10706, 2022.
- M. Heusel, H. Ramsauer, T. Unterthiner, B. Nessler, and S. Hochreiter. GANs trained by a two time-scale update rule converge to a local nash equilibrium. *Advances in neural information processing systems*, 30, 2017.
- J. Horowitz and R. L. Karandikar. Mean rates of convergence of empirical measures in the wasserstein metric. *Journal of Computational and Applied Mathematics*, 55(3):261–273, 1994.
- I. Huh, J. M. Choe, Y. KIM, D. Kim, et al. Isometric quotient variational auto-encoders for structure-preserving representation learning. *Advances in Neural Information Processing Systems*, 36, 2024.
- A. Jacot, F. Gabriel, and C. Hongler. Neural tangent kernel: Convergence and generalization in neural networks. *Advances in neural information processing systems*, 31, 2018.
- T. Karras, T. Aila, S. Laine, and J. Lehtinen. Progressive growing of gans for improved quality, stability, and variation. *CoRR*, abs/1710.10196, 2017. URL <http://arxiv.org/abs/1710.10196>.
- K. Kato, J. Zhou, T. Sasaki, and A. Nakagawa. Rate-distortion optimization guided autoencoder for isometric embedding in Euclidean latent space. In H. D. III and A. Singh, editors, *Proceedings of the 37th International Conference on Machine Learning*, volume 119 of *Proceedings of Machine Learning Research*, pages 5166–5176. PMLR, 13–18 Jul 2020.
- D. Kim, C.-H. Lai, W.-H. Liao, Y. Takida, N. Murata, T. Uesaka, Y. Mitsufuji, and S. Ermon. Pagoda: Progressive growing of a one-step generator from a low-resolution diffusion teacher. *arXiv preprint arXiv:2405.14822*, 2024a.
- J. Z. Kim, N. Perrin-Gilbert, E. Narmanli, P. Klein, C. R. Myers, I. Cohen, J. J. Waterfall, and J. P. Sethna. Gamma-vae: Curvature regularized variational autoencoders for uncovering emergent low dimensional geometric structure in high dimensional data. *arXiv preprint arXiv:2403.01078*, 2024b.

- D. P. Kingma and M. Welling. Auto-encoding variational bayes. In *International Conference on Learning Representations*, 2014. URL <https://openreview.net/forum?id=33X9fd2-9FyZd>.
- M. A. Kramer. Nonlinear principal component analysis using autoassociative neural networks. *AIChE journal*, 37(2):233–243, 1991.
- A. Krizhevsky, G. Hinton, et al. Learning multiple layers of features from tiny images. 2009.
- A. B. L. Larsen, S. K. Sønderby, H. Larochelle, and O. Winther. Autoencoding beyond pixels using a learned similarity metric. In *International conference on machine learning*, pages 1558–1566. PMLR, 2016.
- W. Lee, Y. Yang, D. Zou, and G. Lerman. Monotone generative modeling via a gromov-monge embedding. *arXiv preprint arXiv:2311.01375*, 2023.
- Y. Lee, S. Yoon, M. Son, and F. C. Park. Regularized autoencoders for isometric representation learning. In *International Conference on Learning Representations*, 2022. URL <https://openreview.net/forum?id=mQxt817JL04>.
- X. Li, Z. Qiu, X. Zhao, Z. Wang, Y. Zhang, C. Xing, and X. Wu. Gromov-Wasserstein guided representation learning for cross-domain recommendation. In *Proceedings of the 31st ACM International Conference on Information & Knowledge Management*, pages 1199–1208, 2022.
- S. Lin, S. Roberts, N. Trigoni, and R. Clark. Balancing reconstruction quality and regularisation in elbo for vaes. *arXiv preprint arXiv:1909.03765*, 2019.
- Y. Lipman, R. T. Chen, H. Ben-Hamu, M. Nickel, and M. Le. Flow matching for generative modeling. *arXiv preprint arXiv:2210.02747*, 2022.
- Z. Liu, P. Luo, X. Wang, and X. Tang. Deep learning face attributes in the wild. In *Proceedings of International Conference on Computer Vision (ICCV)*, December 2015.
- A. Makkua, A. Taghvaei, S. Oh, and J. Lee. Optimal transport mapping via input convex neural networks. In *International Conference on Machine Learning*, pages 6672–6681. PMLR, 2020.
- E. Mathieu, T. Rainforth, N. Siddharth, and Y. W. Teh. Disentangling disentanglement in variational autoencoders. In *International conference on machine learning*, pages 4402–4412. PMLR, 2019.
- F. Mémoli. Gromov–Wasserstein distances and the metric approach to object matching. *Foundations of computational mathematics*, 11:417–487, 2011.
- N. Nakagawa, R. Togo, T. Ogawa, and M. Haseyama. Gromov-Wasserstein autoencoders. In *The Eleventh International Conference on Learning Representations*, 2023. URL <https://openreview.net/forum?id=sbS10BCtc7>.

- K. Pandey, A. Mukherjee, P. Rai, and A. Kumar. VAEs meet diffusion models: Efficient and high-fidelity generation. In *NeurIPS 2021 Workshop on Deep Generative Models and Downstream Applications*, 2021.
- G. Peyré, M. Cuturi, and J. Solomon. Gromov-Wasserstein averaging of kernel and distance matrices. In *International conference on machine learning*, pages 2664–2672. PMLR, 2016.
- D. Podell, Z. English, K. Lacey, A. Blattmann, T. Dockhorn, J. Müller, J. Penna, and R. Rombach. Sdxl: Improving latent diffusion models for high-resolution image synthesis. *arXiv preprint arXiv:2307.01952*, 2023.
- R. Rombach, A. Blattmann, D. Lorenz, P. Esser, and B. Ommer. High-resolution image synthesis with latent diffusion models. In *Proceedings of the IEEE/CVF conference on computer vision and pattern recognition*, pages 10684–10695, 2022.
- Y. Song, J. Sohl-Dickstein, D. P. Kingma, A. Kumar, S. Ermon, and B. Poole. Score-based generative modeling through stochastic differential equations. *arXiv preprint arXiv:2011.13456*, 2020.
- A. Srivastava, L. Valkov, C. Russell, M. U. Gutmann, and C. Sutton. Veegan: Reducing mode collapse in GANs using implicit variational learning. *Advances in neural information processing systems*, 30, 2017.
- V. Titouan, R. Flamary, N. Courty, R. Tavenard, and L. Chapel. Sliced Gromov-Wasserstein. *Advances in Neural Information Processing Systems*, 32, 2019.
- A. Vahdat, K. Kreis, and J. Kautz. Score-based generative modeling in latent space. *Advances in neural information processing systems*, 34:11287–11302, 2021.
- A. Van Den Oord, O. Vinyals, et al. Neural discrete representation learning. *Advances in neural information processing systems*, 30, 2017.
- R. Wang, Z. Huang, S. Liu, H. Shao, D. Liu, J. Li, T. Wang, D. Sun, S. Yao, and T. Abdelzaher. Dydiff-VAE: A dynamic variational framework for information diffusion prediction. In *Proceedings of the 44th International ACM SIGIR Conference on Research and Development in Information Retrieval*, pages 163–172, 2021a.
- Y. Wang, D. Blei, and J. P. Cunningham. Posterior collapse and latent variable non-identifiability. *Advances in neural information processing systems*, 34:5443–5455, 2021b.
- H. Xu, D. Luo, and L. Carin. Scalable Gromov-Wasserstein learning for graph partitioning and matching. *Advances in neural information processing systems*, 32, 2019a.
- H. Xu, D. Luo, H. Zha, and L. C. Duke. Gromov-Wasserstein learning for graph matching and node embedding. In *International conference on machine learning*, pages 6932–6941. PMLR, 2019b.
- Y. Yang, W. Lee, D. Zou, and G. Lerman. Improving hyperbolic representations via gromov-wasserstein regularization. *arXiv preprint arXiv:2407.10495*, 2024.